# Flight Delay Prediction via Cross-Modality Adaptation of Large Language Models and Aircraft Trajectory Representation

Thaweerath Phisannupawong<sup>a</sup>, Joshua Julian Damanik<sup>a</sup> and Han-Lim Choi<sup>a,\*</sup>

<sup>a</sup>Department of Aerospace Engineering, Korea Advanced Institute of Science and Technology, 291 Daehak-ro, Yuseong-gu, Daejeon, 34141, Republic of Korea

#### ARTICLE INFO

# Keywords: Flight Delay Prediction Multimodal Models Large Language Models Trajectory Representation Cross-Modality Adaptation

#### ABSTRACT

Flight delay prediction has become a key focus in air traffic management, as delays highlight inefficiencies that impact overall network performance. This paper presents a lightweight large language model-based multimodal flight delay prediction, formulated from the perspective of air traffic controllers monitoring aircraft delay after entering the terminal area. The approach integrates trajectory representations with textual aeronautical information, including flight information, weather reports, and aerodrome notices, by adapting trajectory data into the language modality to capture airspace conditions. Experimental results show that the model consistently achieves sub-minute prediction error by effectively leveraging contextual information related to the sources of delay. The framework demonstrates that linguistic understanding, when combined with cross-modality adaptation of trajectory information, enhances delay prediction. Moreover, the approach shows practicality and scalability for real-world operations, supporting real-time updates that refine predictions upon receiving new operational information.

# 1. Introduction

The volume of air traffic grows in parallel with economic development. This growth can result in traffic density that exceeds the capacity of current air traffic management (ATM) systems, compromising both safety and operational efficiency [1, 2]. Such inefficiencies lead to flight delays that increase airline operating costs, burden airport coordination, disrupt passenger itineraries, and create network-wide ripple effects. The Federal Aviation Administration (FAA) defines delay as the excess time duration incurred during flight operations. These delays are divided into five operational phases, namely gate delay, taxi-out delay, en-route delay, terminal delay, and taxi-in delay [3]. Delays can also be classified by cause, including carrier delays, weather delays, security delays, and airspace-related delays [4]. The delays across operational phases and causes originate from different parts of the ATM system. Understanding relevant factors is essential for accurate, phase-specific delay prediction. This study focuses on delays after the terminal phase, which are of particular interest to air traffic controllers (ATCs), as monitoring and mitigating delays within this phase is their direct responsibility.

In ATM operations, the ATCs monitor trajectory data and textual aeronautical information, which belong to different modalities. Although these data are comprehensively human-interpretable, managing, inferring, and making decisions based on large volumes of such multi-modal information can still be overwhelming for ATCs. The growing public availability of large-scale aviation data has enabled the development of data-driven models to assist ATCs in these tasks, enhancing autonomy while preserving effective human-machine interaction. Textual information, such as flight schedules, weather reports, weather forecasts, and temporary operational notices, provides essential context for aviation operations and is nowadays accessible via many public databases. Aircraft trajectory data, which describes aircraft movement and operational behavior within controlled airspace, can be extracted from recorded Automatic Dependent Surveillance—Broadcast (ADS-B) databases. Integrating and understanding these contexts plays an important role in improving airspace-related delay prediction.

Since the operational context comprises information in different modalities, each requires distinct handling techniques, while their combined use requires effective data integration. For textual data, large language models (LLMs) have recently gained recognition as powerful models capable of understanding natural language. Pretrained on large-scale language corpora, LLMs can often interpret aviation-related text, such as flight descriptions and aeronautical

<sup>\*</sup>Corresponding author

<sup>🗟</sup> petchthwr@kaist.ac.kr (T. Phisannupawong); joshuad@kaist.ac.kr (J.J. Damanik); hanlimc@kaist.ac.kr (H. Choi)
ORCID(s):

information. On the other hand, trajectories are complex, high-dimensional time series that can be represented in a more compact form, which helps downstream models perform better even without further fine-tuning. However, trajectory data is not the type of input recent LLMs are trained to handle directly; therefore, integrating such data with LLMs requires additional adaptation techniques. This paper's proposed method incorporates two pre-trained models, an LLM and a trajectory representation model, using a simple yet effective adaptation technique to integrate their embeddings. We formulate flight delay prediction as a multimodal regression problem, where both textual and trajectory data serve as inputs for prediction. The contributions of this paper are as follows:

- We propose a language-trajectory multimodal framework for predicting delays beyond the terminal phase, incorporating comprehensive operational context through the integration of textual aeronautical information and aircraft trajectories, leveraging an LLM and a trajectory representation model for their respective modalities.
- This paper uncovers that the linguistic understanding embedded in pretrained LLMs is crucial and can be effectively transferred and adapted to the flight delay prediction task, highlighting their potential for efficient multimodal inference without requiring computationally intensive full fine-tuning.
- We demonstrate that incorporating a wide range of aeronautical information into the operational context leads to more accurate delay predictions, as the model can account for contextual factors that describe the situation in the airspace, which in turn extend the time an aircraft spends within the area.
- Our framework supports real-time delay monitoring by processing continuously updated inputs, such as surveillance broadcast signals, enabling second-by-second updates that are useful for operators who require more frequent real-time updates as the aircraft approaches the airport.

# 2. Related Works

# 2.1. Delay Prediction

Flight delay prediction has long been an area of interest in the ATM community. Early studies employed tabular-based approaches, in which flight details (e.g., carrier, route, schedule, delay history) and contemporaneous weather data (e.g., visibility, wind, temperature) were extracted into structured tables and used as fixed-dimensional numerical or categorical features for machine learning models. Delay prediction can be formulated as a classification problem, where the goal is to determine whether a delay will occur. For example, prior studies have employed logistic regression [5] and a modified Random Forest model [6]. Meanwhile, [7–10] have compared various non-neural machine learning models for delay classification. Integrating traffic count features, [11] predicts departure delays using linear regression, support vector machines (SVM), Multilayer Perceptron (MLP), and LightGBM. The delay prediction can also be formulated as a regression problem that predicts delay duration in minutes. For example, SVM [12] and an MLP using only flight information [13] have been applied to predict delay duration. [14] compares several models for predicting delay distributions from flight features; subsequently, [9, 15, 16] compare various models for delay regression.

Many works have incorporated historical data for delay classification in sequence. For instance, [17, 18] both employ long short-term memory (LSTM) models using flight information and weather data to classify next-day delay. However, the day-level granularity in both limits their real-time applicability. Complex network models, such as the LSTM-integrated random forest model [19] and the Convolutional Neural Network–Long Short-Term Memory (CNN-LSTM) [20], were employed to predict delays based on weather, delay propagation, and airport congestion, as measured by traffic count. [21] models multi-flight delay propagation using attention-based architectures that capture flight chain dependencies across sequential operations of the same aircraft, accounting for temporal coupling and propagation effects in aircraft rotations. [4] employs Gaussian Process Regression to predict flight delays using only the prior delays and flight dates, with the model learning the mean and covariance from historical delay patterns.

Several recent studies have adopted graph-based approaches for delay regression. [22] employs a GCN-CNN architecture, where a Graph Convolutional Network (GCN) captures spatial dependencies in a time-evolving network of airports, and a CNN models daily and weekly delay patterns. Similarly, [23] proposes a hybrid framework that combines diffusion GCNs with residual Gated Recurrent Units (GRUs), incorporating federated learning across airport networks for accurate, privacy-preserving forecasting using historical delay data. [24] represents air traffic as a directed multigraph for predicting delays caused by holding maneuvers. [25] employs an attention-based LSTM model combining aircraft trajectory with flight and weather data to classify delays as early, on-time, or late.

Table 1
Comparison of Prediction Contexts and Formulations in Delay Prediction Models

				Prediction	Context				Formu	Formulation	
Method	Flight Info	Wea	ather	NOTAMs	Traje	ctory Dat	a	Airport Corr.	Classif.	Regr.	
		Current	Forecast		Focusing	Active	Prior				
Tabular-Based Models											
Linear Regression [15, 16]	num	num	-	-	-	-	-	-	-	1	
Logistic Regression [5, 7, 8, 10]	num	num	-	-	-	-	-	_	✓	-	
Decision Tree [7, 10, 16]	num	num	-	-	-	-	-	_	✓	1	
Random Forest [6-10, 14, 16]	num	num	-	-	-	-	-	-	✓	1	
KNN [7]	num	num	-	-	-	-	-	-	✓	-	
SVM [7, 12, 16]	num	num	-	-	-	-	-	-	✓	1	
Naïve Bayes [7, 8, 10]	num	num	-	-	-	-	-	-	✓	-	
Gradient Boosting [7–9, 14, 16]	num	num	-	=	-	-	-	-	✓	1	
MLP [8, 9, 13, 14]	num	num	-	=	-	-	-	-	✓	1	
LR/SVM/MLP/LGBM [11]	num	num	-	-	num*	num*	-	-	✓	-	
Sequential Models											
LSTM [17, 18]	seq	seq	-	-	-	-	-	-	✓	-	
ST-Random Forest [19]	seq	seq	-	-	seq*	seq*	-	seq	✓	-	
CNN-LSTM [20]	seq	seq	-	-	seq*	seq*	-	seq	✓	-	
CBAM [21]	seq	-	-	-	-	-	-	-	✓	-	
Gaussian Process [4]	seq	-	-	-	-	-	-	-	-	✓	
Graph-based Models											
GCN-CNN [22]	graph-seq	-	-	-	-	-	-	graph-seq	-	1	
GCN-GRU [23]	graph-seq	-	-	-	-	-	-	graph-seq	-	1	
GATs [24]	graph	-		-	-		-	graph	✓		
Trajectory-Based Models											
LSTM-Attention [25]	num	num	-	-	ts	-	-	-	✓	-	
Ours	txt	txt	txt	txt	ts	ts	ts	-	-	1	

Abbreviations: num = fixed-dimensional numerical/categorical tabular features, seq = sequence of numerical features, ts = raw time-series trajectory, txt = textual data, graph = graph-structured data, graph-seq = sequence of graph-structured data. \*Only trajectory count, disregard full trajectory information.

#### 2.2. Large Language Models

The Transformer architecture [26] has introduced powerful contextualization and has become the foundation for most subsequent language models. Pretrained language models began with GPT-1 [27, 28], which used generative pretraining with a causal decoder-only Transformer. BERT [29] introduced masked language modeling and next sentence prediction with a bidirectional encoder, while T5 [30] employed an encoder-decoder architecture for text-to-text tasks on the C4 corpus. The LLM was further advanced by GPT-3 [31], which demonstrated strong few-shot prompting without task-specific fine-tuning. This approach is now widely adopted in research and applications, along with techniques such as instruction tuning [32] for improved prompt-following and Reinforcement Learning from Human Feedback (RLHF) [33]. With these techniques, models such as GPT-3.5, GPT-4, GPT-40, Gemini, Claude, and DeepSeek V3 were released and remain proprietary, serving as high-performing models for research and industry applications. Open-source LLMs have been released, enabling broader access within the communities, including Meta's LLaMA series [34–36], Mistral-7B and Mixtral-8x7B [37, 38], Google's Gemma series [39–41], Microsoft's Phi models [42–44], the Qwen family [45–49], and DeepSeek-R1 [50]. These models achieve performance comparable to proprietary ones and unlock new possibilities for customization and specialized use through flexible adaptation.

#### 2.3. Time Series and Multimodal Models

Given that trajectories are inherently time series, the development of time-series pretrained models, also referred to as time-series representation learning, can be traced back to the autoencoder [51], which is widely used in the ATM field. The encoder is trained to compress input sequences, and the decoder is trained to reconstruct the original data. Contrastive representation learning aligns similar samples in the embedding space while separating dissimilar ones. Notably, recent works include TS2Vec [52], which employs hierarchical contrastive learning between two randomly masked views; TF-C [53], which aligns time-based and frequency-based views; SimMTM [54], which utilizes masked time-series modeling; and InfoTS [55], which leverages meta-learning for data augmentation method selection. Aircraft

Trajectory Segmentation-based Contrastive Coding (ATSCC) [56] is a framework for aircraft trajectory data that ensures consistent embedding of cumulative trajectory information within segments. It generates high-fidelity instance-level representations that outperform prior methods in instance-level tasks such as classification and clustering, with embeddings that align closely with human-defined aeronautical procedures.

LLMs and Large Multimodal Models (LMMs) for time series are rapidly growing research areas. Cross-modality adaptation is a powerful technique for leveraging pretrained models from one modality and adapting them for use in other modalities. LLM4TS [57] proposed a two-stage fine-tuning, where an LLM is first pretrained to align with the time-series modality, and then further fine-tuned on a forecasting task. LLMTIME [58] demonstrated a procedure for tokenizing continuous-valued time series into discrete tokens, enabling the direct use of pretrained LLMs for time series forecasting. Time-LLM [59] introduces a reprogramming layer that converts time series into LLM-friendly embeddings, combined with a prompt-as-prefix strategy and a trainable projection layer on top of a frozen LLM.

# 2.4. Large Language Model for Aviation Applications

LLM applications have extended to aviation-related language tasks. AviationGPT [60] fine-tuned and instructiontuned LLMs on an aviation corpus comprising books, documents, and textual data such as METAR (Meteorological Aerodrome Reports), TAF (Terminal Aerodrome Forecasts), and NOTAM (Notice to Airmen). Aviation-BERT [61] was pretrained using MLM on reports from the Aviation Safety Reporting System and the National Transportation Safety Board. AeroBERT [62, 63] was introduced for classification and named entity recognition on engineering requirements. In [64], GPT-3.5-Turbo was fine-tuned to predict means of compliance for aerospace systems. CHATATC [65] was fine-tuned on Ground Delay Program data to be a conversational agent. LLMs have also been applied to various ATM tasks. In [66], GPT-40 was fed with auto-generated flight planning prompts, wind hazard polygons, and operator preferences to generate route recommendations, which are then verified by the operator. The work in [67] presented supervised fine-tuning of LLMs, enabling the generation of conflict-free flight slot allocation. The ATM agents in [68] use a dual LLM-based framework that interacts with the BlueSky [69] simulator to monitor traffic, interpret situations, and generate conflict-minimized instructions. The application of LLMs for trajectory data has also been explored in recent works. FlightBERT [70] uses a bidirectional MTM to learn representations for flight trajectory prediction. FlightBERT++ [71] extends this to support additional downstream tasks, including anomaly detection and intent classification. The study in [72] fine-tunes the LLM on a text-reformatted prompt-based trajectory dataset. The work in [73] fine-tunes LLaMA to reconstruct aircraft positional states from incomplete sequences. SIA-FTP [74] integrates ATC speech and flight trajectory data by using BERT for text and FlightBERT++ for trajectories, fusing their representations for trajectory prediction.

# 3. Methodology

# 3.1. Problem Formulation

Considering a flight with identifier *i*, the time horizon of its entire operation is illustrated in Figure 1. Generally, the key temporal markers that define the operational timeline of a flight include the scheduled and actual departure times, airborne time, airspace entry time, landing time, and arrival time. As described in [3], delay can be decomposed into components corresponding to each phase of flight operations. As shown in Figure 1, the total delay is the accumulation of delays that occur during each phase of the flight. In this paper, we define the pre-terminal phase as all operations prior to entering the airspace. Accordingly, the pre-terminal delay consists of gate delay, taxi-out delay, and enroute delay. Gate delay may result from service-related operations, delay of previous flights, or other logistical factors. Taxi-out delay is commonly caused by ground holding procedures. Enroute delay is influenced by factors such as adverse enroute weather conditions and required detours. These components can be rearranged as follows:

$$D_{pre} = D_{gate} + D_{taxi-out} + D_{enroute} \tag{1}$$

$$D_{pre} = D_{gate} + D_{taxi-out} + \left(T_{entry}^{act} - T_{entry}^{exp} - D_{gate} - D_{taxi-out}\right)$$
 (2)

$$D_{pre} = T_{entry}^{act} - T_{entry}^{exp} \tag{3}$$

We define the post-terminal phase as the operations of aircraft after entering the airspace. The post-terminal delay encompasses terminal delay and taxi-in delay. Terminal delay typically arises from air traffic congestion, weather disruptions, or airspace restrictions. Taxi-in delay is generally attributed to ground congestion at the destination airport.

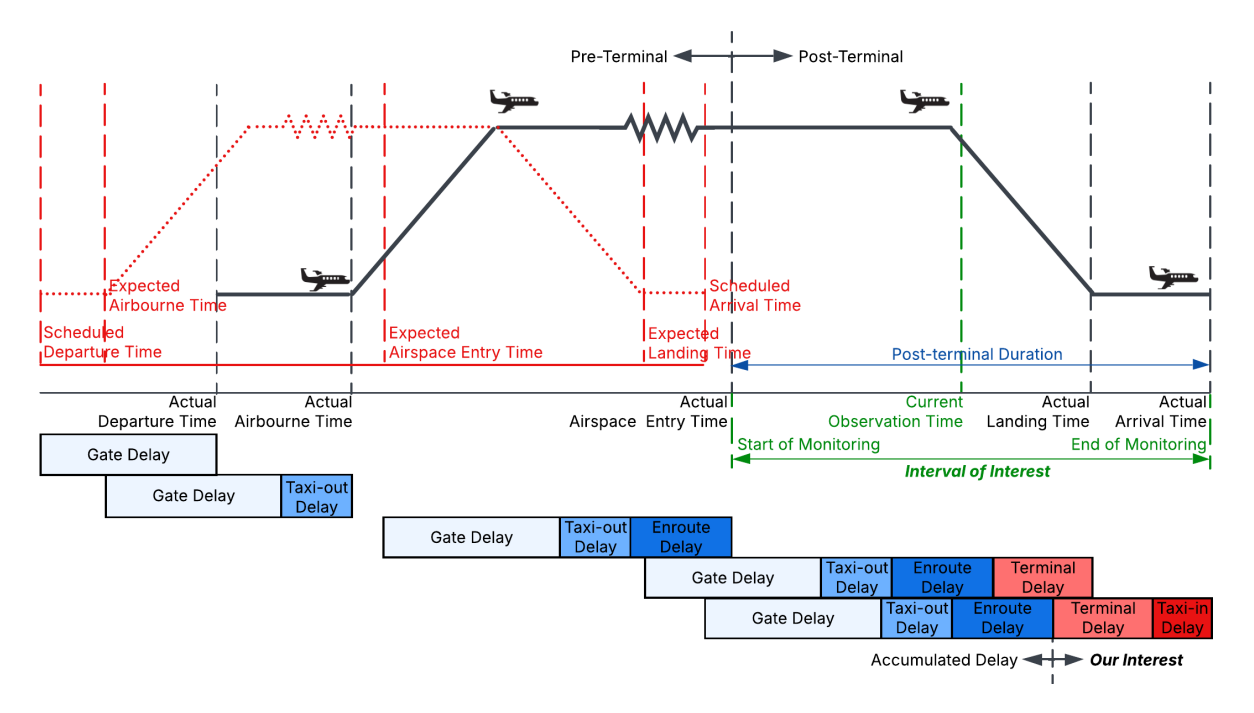


Figure 1: Flight Delay Accumulation of Aircraft Operations from Departure to Arrival

These delay components can be rearranged as follows:

$$D_{post} = D_{terminal} + D_{taxi-in} \tag{4}$$

$$D_{post} = \left(T_{land}^{act} - T_{land}^{exp}\right) - \left(T_{entry}^{act} - T_{entry}^{exp}\right) + \left(T_{arr}^{act} - T_{arr}^{sch}\right) - \left(T_{land}^{act} - T_{land}^{exp}\right) \tag{5}$$

$$D_{post} = \left(T_{arr}^{act} - T_{arr}^{sch}\right) - \left(T_{entry}^{act} - T_{entry}^{exp}\right) \tag{6}$$

Thus, the total delay is defined as the sum of delays accumulated during both the pre-terminal and post-terminal phases. This paper's problem formulation is designed from the perspective of an ATC at the destination airport, who is responsible for monitoring aircraft within a designated control area. This involves tracking and updating delay information from the actual airspace entry time  $T_{entry}^{act}$  until the actual arrival time  $T_{arr}^{act}$ . Since the scheduled arrival time is known, and  $T_{entry}^{act}$  marks the start of monitoring, parts of the delay can be inferred from these known values.

$$D_{total} = D_{pre} + D_{post} \tag{7}$$

$$D_{total} = \left(T_{entry}^{act} - T_{entry}^{exp}\right) + \left(T_{arr}^{act} - T_{arr}^{sch}\right) - \left(T_{entry}^{act} - T_{entry}^{exp}\right) \tag{8}$$

$$D_{total} = T_{entry}^{act} - T_{arr}^{sch} + \left(T_{arr}^{act} - T_{entry}^{act}\right) \tag{9}$$

$$D_{total} = T_{entry}^{act} - T_{arr}^{sch} + \Delta t_{post}$$
 (10)

The post-terminal duration is denoted as  $\Delta t_{post}$ . This value remains unknown during the monitoring period at the current observation time  $t \in \left[T_{entry}^{act}, T_{arr}^{act}\right]$  because  $T_{arr}^{act}$  has not yet been observed. Thus, we aim to estimate  $\Delta t_{post}$  using available contextual information. Unlike the graph-based and sequential models in Table 1, the past delays are accumulated in the gate delay for a particular flight, the component known to the ATC at the destination airport, and those terms are eliminated in our pre-terminal delay formulation in equation 3, leaving only the post-terminal duration  $(\Delta t_{post})$  to be predicted. Accordingly, the estimated total delay is given by:

$$\hat{D}_{total} = T_{entry}^{act} - T_{arr}^{sch} + \Delta \hat{t}_{post}$$
 (11)

The advantage of predicting the post-terminal duration is that it typically aligns with maneuvering procedures, as similar procedures usually result in similar durations; however, variations can still occur due to various factors. We hypothesize that accurate prediction of  $\Delta \hat{t}_{post}$  requires the integration of flight information, weather conditions, non-periodic operational events, and traffic congestion. Therefore, comprising the most comprehensive context compared in Table 1, we define a scenario  $s_{i,t}$  of the flight i at time t that consists of textual prompts that include general flight information, weather information, NOTAMs, and airspace conditions described by aircraft trajectories. Such that,

$$s_{i,t} = \left\{ P_{i,t}^{fp}, P_t^{wx}, P_t^{no}, X_{i,t}^f, X_{i,t}^a, X_{i,t}^p \right\}$$

$$P_{i,t}^{fp}, P_t^{wx}, P_t^{no} \in \mathbb{Z}^{L_i^{(j)}}, \quad j \in \{fp, wx, no\}$$

$$X_{i,t}^f, X_{i,t}^a, X_{i,t}^p \in \mathbb{R}^{N^{(k)} \times \mathcal{T}_{\max}^{(k)} \times 3}, \quad k \in \{f, a, p\}$$

$$(12)$$

A scenario,  $s_{i,t}$ , comprises data from multiple modalities. The textual prompt  $P_t^{fp}$  encodes general flight information,  $P_t^{wx}$  captures weather conditions by combining METAR and TAF reports, and  $P_t^{no}$  contains NOTAMs information. This paper introduces a trajectory-based characterization of airspace conditions, enabling the model to interpret congestion more effectively than the traffic count methods used in [11, 19, 20]. The trajectory data is represented as a time-series modality, where each timestep contains the x, y, z coordinates in the ENU (East-North-Up) frame. To describe the airspace, we use three distinct groups of trajectories. The focusing trajectory  $X_{i,t}^f$ , the active trajectories  $X_{i,t}^a$  those currently airborne at time t, and the completed prior trajectories  $X_{i,t}^p$ , which may provide additional context or relevant information. The prediction model is formulated as  $\hat{y}_i = f_{\theta}(s_{i,t})$ , where  $\hat{y}_i \equiv \Delta \hat{t}_{post,i}$ , and the two notations are used interchangeably. The function  $f_{\theta}$  represents the overall model, composed of several components. The text part includes a tokenizer  $T(\cdot)$ , followed by an embedding table Emb[·]. The trajectory part consists of the ATSCC representation network, denoted as  $f_{\text{atscc}}(\cdot)$  [56], followed by a trainable cross-modality adaptation network  $f_{\text{xa}}(\cdot)$ . The combined embeddings are then passed to a frozen LLM backbone  $f_{\text{llm}}(\cdot)$ . Finally, a trainable prediction head  $f_h(\cdot)$  that predicts  $\hat{y}_i$ . The training of the model  $f_{\theta}(\cdot)$  is formulated as a regression problem, minimizing the error between the predicted post-terminal duration  $\hat{y}_i$  and the ground-truth  $y_i$ .

#### 3.2. Dataset Preparation

The model training requires ground-truth pairs  $(y_i, s_{i,t})$ , where  $y_i$  denotes the actual post-terminal duration, and  $s_{i,t}$  represents the multimodal input scenario. Monthly datasets are compiled for flights arriving at Incheon International Airport throughout 2022. To construct these datasets, we integrate information from multiple sources, including flight schedules, aircraft trajectories, meteorological data, and NOTAMs, resulting in a comprehensive multimodal collection for delay prediction.

#### 3.2.1. General Flight Information Processing

We first construct a flight schedule database using data on arrival flights at Incheon International Airport for the year 2022, queried from Airportal [75]. The retrieved records consist of structured information, including scheduled arrival times, airline names, flight identifiers, and airport details such as departure and destination codes, as well as airport names. We matched the airports with their coordinates, including latitude, longitude, and altitude, and calculated the great-circle distance between the origin and destination. The flight haul type, categorized as short-haul, medium-haul, or long-haul, is determined based on this distance according to the classification provided in Wragg's aviation dictionary [76]. The date and day of the week of arrival are recorded in Korea Standard Time. Certain fields are synthesized to complete the dataset. Aircraft type and registration are inferred based on the frequently used aircraft models on each specific route. The wake turbulence category is classified based on the aircraft type in accordance with ICAO's Procedures for Air Navigation Services - Air Traffic Management Doc 4444 [77]. The actual airspace entry time and the current time stamp (t) are included here to provide additional context. Each flight t is associated with general flight information, as detailed in Table 2, which is later used to construct the prompt  $P_{t,t}^{fp}$  using the format in Figure 9.

#### 3.2.2. Textual Data Preprocessing

Since METARs, TAFs, and NOTAMs are provided in aeronautical coded text formats, we deliberately use their original, non-decoded forms to emphasize a key strength that the framework does not require separate decoders for

Table 2
General Flight Information Data Descriptions and Data Types

Flight Information	Description	Data Type
airline_name_english	Airline name in English	string
callsign_code_iata	IATA-format callsign	string
callsign_code_icao	ICAO-format callsign	string
haul	Flight haul type (short, medium, long, local)	string
dep_code_iata	Departure airport IATA code	string
dep_code_icao	Departure airport ICAO code	string
dep_name_english	Departure airport name	string
dep_lat	Departure airport latitude	float64
dep_lon	Departure airport longitude	float64
dep_altitude	Departure airport altitude (ft)	float64
dest_code_iata	Destination airport IATA code	string
dest_code_icao	Destination airport ICAO code	string
dest_name_english	Destination airport name	string
dest_lat	Destination airport latitude	float64
dest_lon	Destination airport longitude	float64
dest_altitude	Destination airport altitude (ft)	float64
distance	Great-circle distance between origin and destination (km)	float64
actual_entry_time	Time of first ADS-B appearance or airspace entry	datetime64
sched_time_utc	Scheduled arrival time (UTC)	datetime64
date	Scheduled Flight Date of arrival (KST)	datetime64
day_of_week	Scheduled Day of week of arrival (KST)	string
aircraft_type	Aircraft type	string
$aircraft\_registration$	Aircraft registration code	string
wake_turbulence_cat	Wake turbulence category	string

these coded texts. Spanning the entire year of 2022, the METARs and TAFs were mass-downloaded from Ogimet [78], while NOTAMs were collected from the AIM Korea [79]. The active time periods of the coded texts vary by source. For a time t, the METAR report is retrieved by selecting the one whose release time falls within the preceding 30-minute update interval. In contrast, TAFs and NOTAMs explicitly define their active periods. TAF reports are typically issued every six hours, and multiple forecasts may overlap at a given time; therefore, we select the most recent valid TAF. For NOTAMs, multiple notices can be concurrently active, so we collect all active NOTAMs. The prepared METAR, TAF, and NOTAMs, at time t, are directly used to construct the prompts,  $P_t^{uv}$  and  $P_t^{no}$ , as in Figure 10 and Figure 11.

#### 3.2.3. Trajectory Data Preprocessing

The ADS-B data were sourced from the OpenSky database [80]. The data for both arrival and departure flights spanning the entire year of 2022 were queried using flight identification numbers from the Airportal website [75]. We extracted positional states from the surveillance data, including latitude, longitude, and barometric altitude. Barometric altitude was chosen for its lower noise levels and greater reliability compared to GPS vertical accuracy [81]; moreover, it is commonly used for traffic control. The positional features were transformed into ENU coordinates centered at the airport. The trajectories were resampled to 1-second intervals without interpolating into a fixed number of timestamps. Each trajectory was scaled by dividing by 120 kilometers, following the reproduction details in [56]. A preprocessed trajectory of flight i consists of states  $x_{i,t} = \{x_{i,t}^x, x_{i,t}^y, x_{i,t}^z\}$  over all recorded timestamps since its airspace entry. There are three types of trajectories: the focusing trajectory, active trajectories, and prior trajectories. Their temporal relationships are illustrated in Figure 2, and their definitions in a scenario  $s_{i,t}$  are as follows:

- Focusing trajectory: The trajectory of the flight i, comprising the states from its first ADS-B transmission in the airspace up to the current time t. It explains the current status and prior states of the focusing aircraft. The focusing trajectory is denoted as  $X_{i,t}^f \in \mathbb{R}^{1 \times \mathcal{T}^f \times 3}$ , where  $T^f$  is the number of trajectory states recorded from the aircraft's first appearance in the airspace up to the current time t.
- Active trajectories: The trajectories of other aircraft operating in the terminal maneuvering area (TMA) at time t, excluding the focusing flight i. This type of trajectory provides insight into the current airspace condition and congestion, similar to how an air traffic controller monitors multiple aircraft simultaneously. Each active

trajectory contains states from the time the aircraft departed or first entered the TMA up to time t. The active trajectories are nan-padded and denoted as  $X_{i,t}^a \in \mathbb{R}^{N^a \times \mathcal{T}_{\max}^a \times 3}$ , where  $N^a$  is the number of active trajectories at time t, and  $\mathcal{T}_{\max}^a$  is the maximum trajectory length among all active trajectories.

• Prior trajectories: Using the earliest timestamp among all active trajectories as a reference point, we collect all completed prior trajectories that were active at that time. Although these flights have completed their operations, they may still hold semantic importance. They capture patterns that may influence the paths of focusing and active flights, such as when aircraft are instructed to follow earlier ones. They also indirectly visualize ground traffic activity. The prior trajectories are nan-padded and represented as X<sup>p</sup><sub>i,t</sub> ∈ ℝ<sup>N<sup>p</sup>×T<sup>p</sup><sub>max</sub>×3</sup>, where N<sup>p</sup> denotes the number of prior trajectories at time t, and T<sup>p</sup><sub>max</sub> is the longest trajectory length among them.

Therefore, the trajectories  $X_{i,t}^f$ ,  $X_{i,t}^a$ , and  $X_{i,t}^p$  represent the query at time t for flight i under scenario  $s_{i,t}$ . Intuitively, these trajectories enable the model to achieve a comprehensive semantic understanding of the airspace, akin to the mental image used by human ATCs, without requiring explicit procedures such as trajectory classification or waypoint capacity estimation. This allows the model to directly perform the target task, estimating the post-terminal duration.

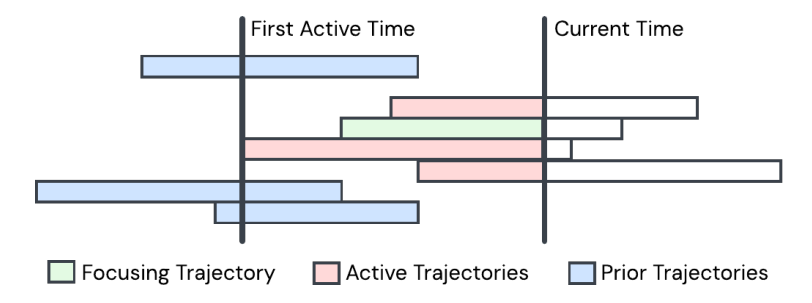


Figure 2: Temporal Relationship Between Focusing, Active, and Prior Trajectories

#### 3.2.4. Label Preparation

The corresponding label  $y_i$  for the regression task associated with  $s_{i,t}$  was constructed as part of the supervised training setup. For flight i, the actual post-terminal duration, denoted as  $\Delta t_{post,i}$ , is calculated using the airspace entry time  $T_{entry,i}^{act}$ , derived from ADS-B data [80], taken as the moment the aircraft enters Incheon Airport's TMA, and the actual arrival time  $T_{arr,i}^{act}$ , obtained from the official records in hour–minute format in Airportal [75]:

$$y_i \equiv \Delta t_{post} = T_{arr}^{act} - T_{entry}^{act}. \tag{13}$$

As a result, we obtain a multimodal dataset comprising general flight information in structured form, weather reports and NOTAMs in textual form, and trajectories as time-series data. Each component is integrated into  $s_{i,t}$ , which is then paired with a regression label  $y_i$  representing the actual post-terminal duration. We repeat the preparation procedure for all flights i within each month, selecting min $(5, T_i)$  time points per flight, where  $T_i$  is the number of recorded states of flight i, to construct 12 datasets corresponding to each month spanning the year 2022. For each dataset, the most recent 10% are reserved as the testing set, another 10% is randomly sampled for validation, and the remaining scenarios are used for training. The visualization in Figure 3 illustrates the number of flights and the data size in each dataset.

#### 3.3. Neural Network Architecture

This section outlines the architecture of the proposed multimodal regression model  $f_{\theta}(s_{i,t})$ . This section describes how structured natural language prompts, derived from flight information, weather reports, and NOTAMs, as well as time-series trajectory data, are individually embedded. We also explain how a cross-modality adaptation network aligns trajectory and language embeddings, enabling seamless multimodal integration for predicting post-terminal duration through a regression head that replaces the LLM's original language modeling head.

#### 3.3.1. Natural Language Prompt Embedding

To process natural language inputs, including prompts for general flight information, weather information, and NOTAMs, we utilize the tokenizer and embedding table provided by the selected LLM. We denote the tokenizer

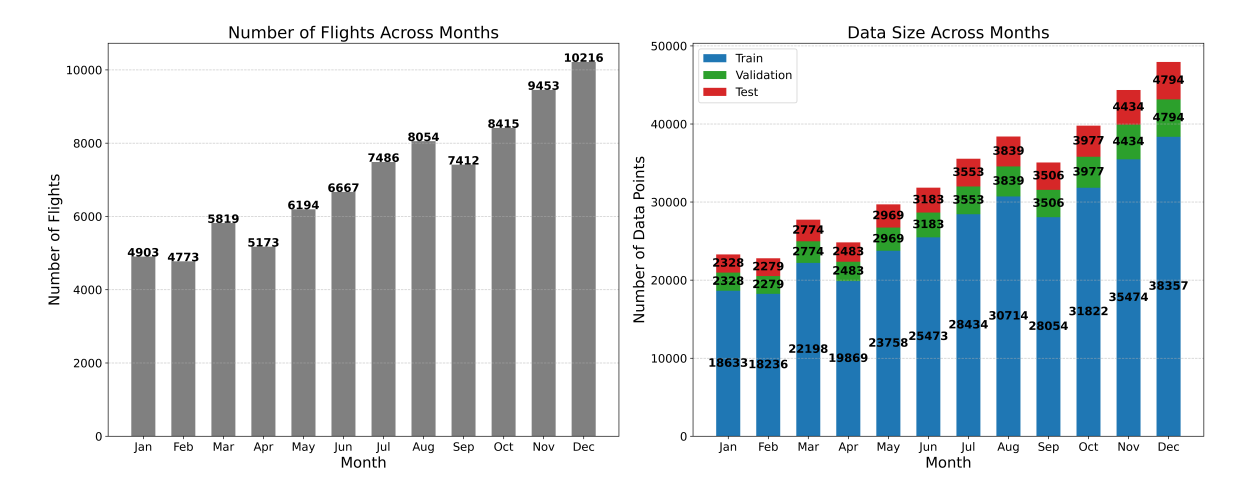


Figure 3: Dataset Statistics

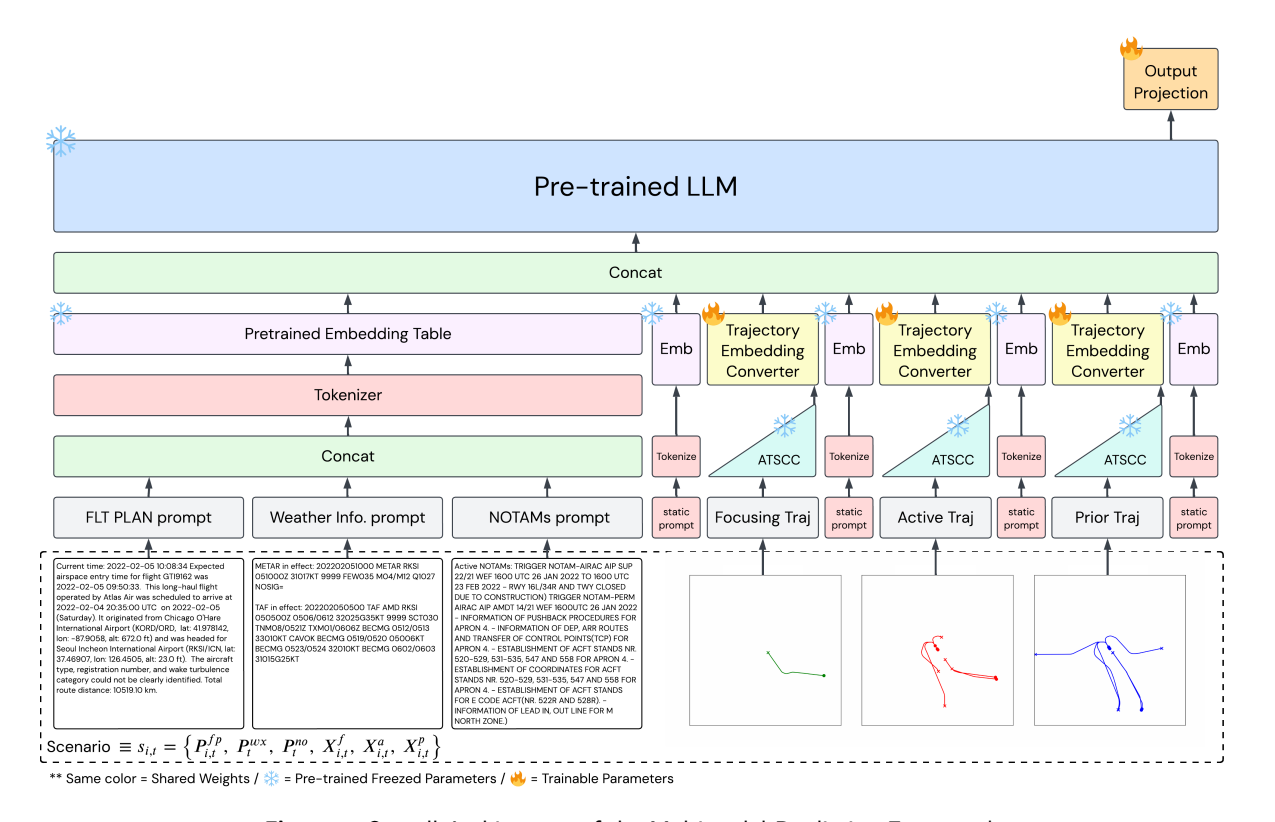


Figure 4: Overall Architecture of the Multimodal Prediction Framework

as a function  $T(\cdot)$ , which transforms each combined prompt  $P_{i,t}$ , where  $P_{i,t} = P_{i,t}^{\mathrm{fp}} \parallel P_t^{\mathrm{wx}} \parallel P_t^{\mathrm{no}}$ , into a sequence of subword tokens. The resulting tokenized sequence is  $T(P_{i,t}) = [p_1, p_2, \dots, p_L]$ , where L denotes the length of the token sequence. Each token  $p_l \in T(P_{i,t})$  is then mapped to a continuous embedding vector  $\mathbf{z}_l^p \in \mathbb{R}^d$  using the pretrained embedding table  $\mathrm{Emb} \in \mathbb{R}^{V \times d}$ , where V is the vocabulary size and d is the embedding dimension. The output of this step is the embedded prompt representation:

$$\mathbf{Z}_{i,t}^{p} = \operatorname{Emb}[T(P_{i,t})] \tag{14}$$

where  $\mathbf{Z}_{i,t}^p \in \mathbb{R}^{L \times d}$  is the token-level embedding sequence for prompt  $P_{i,t}$ . The embedding table and tokenizer are kept fixed during training to preserve the pretrained language understanding, ensuring that natural language inputs are represented consistently and remain aligned with the pretrained LLM.

#### 3.3.2. Trajectory Representation Model

The three trajectory types, focusing  $X_{i,t}^f$ , active  $X_{i,t}^a$ , and prior  $X_{i,t}^p$ , are time-series data compressed into instance-level representations using a pretrained trajectory encoder, where each embedding represents one trajectory. Thus, it is crucial that each embedding preserves the semantic fidelity of its corresponding trajectories and aligns well with human understanding of air traffic patterns. ATSCC [56] is well-suited for air traffic trajectory data, showing strong performance in instance-level tasks like classification and clustering, with representations that align with aeronautical procedures without relying on predefined labels. Therefore, the trajectory representation encoder model  $f_{atscc}(\cdot)$  follows the architecture and was pretrained in accordance with the reproduction details of ATSCC.

We reproduce the trajectory encoder by strictly following the reproduction details of the ATSCC framework [56]. The causal transformer encoder architecture features 12 layers with a model dimension of 768, feed-forward network dimensions of 3072 using the Gaussian Error Linear Unit (GELU) activation, and 12 attention heads. The model has an input projection from 9 to the model dimension and an output projection from the model dimension to 320. ATSCC follows the NoPos [82], which omits positional encoding. Additionally, L2 normalization is applied after both input and output projections. The model is pre-trained on ATFMTraj [83] data, using 5-second interval downsampling and combining both Incheon departures and arrivals. To enhance the expressiveness of trajectory data, additional geometric features, including direction vectors and polar coordinates, are computed. For each timestep k in a time-series instance, the additional geometric features are calculated as:

$$\{x_{i,k}^{u_x}, x_{i,k}^{u_y}, x_{i,k}^{u_z}\} = \frac{x_{i,k+1} - x_{i,k}}{\|x_{i,k+1} - x_{i,k}\|},\tag{15}$$

$$\{x_{i,k}^{r}, x_{i,k}^{\sin \theta}, x_{i,k}^{\cos \theta}\} = \left\{ \sqrt{\left(x_{i,k}^{x}\right)^{2} + \left(x_{i,k}^{y}\right)^{2}}, \sin\left(\arctan 2(x_{i,k}^{y}, x_{i,k}^{x})\right), \cos\left(\arctan 2(x_{i,k}^{y}, x_{i,k}^{x})\right) \right\}. \tag{16}$$

$$x_{k} = \{x_{i,k}^{x}, x_{i,k}^{y}, x_{i,k}^{z}, x_{i,k}^{u_{x}}, x_{i,k}^{u_{y}}, x_{i,k}^{u_{z}}, x_{i,k}^{r}, x_{i,k}^{\sin \theta}, x_{i,k}^{\cos \theta}\}$$

$$(17)$$

During pretraining, we apply a dropout rate of 0.35 and binomial input embedding masking with a probability of 0.2. The model is trained using the AdamW optimizer with a batch size of 16, a learning rate of  $1 \times 10^{-5}$ , and weight decay of  $1 \times 10^{-5}$ . A grid search is conducted by separating a small portion of the dataset for validation to determine the optimal segmentation threshold and contrastive loss temperature based on classification and clustering performance. After pretraining, the trajectory encoder weights are frozen and not updated further.

The pre-trained encoder, denoted as  $f_{\mathrm{atscc}}(\cdot)$ , first applies geometric extraction functions to  $X_{i,t}^{(k)} \in \mathbb{R}^{N^{(k)} \times \mathcal{T}_{\mathrm{max}}^{(k)} \times 3}$  to expand each trajectory state into a 9-dimensional feature vector  $X_{i,t}^{(k)} \in \mathbb{R}^{N^{(k)} \times \mathcal{T}_{\mathrm{max}}^{(k)} \times 9}$  with 5-second interval downsampling, followed by input projection and a forward pass through the causal transformer backbone. The final timestep output is then linearly projected to a 320-dimensional instance-level representation. The process of encoding the trajectory for type k is illustrated in Figure 5 and formally defined as

$$Z_{i\,t}^{(k)} = f_{\text{atscc}}(X_{i\,t}^{(k)}),\tag{18}$$

where  $k \in \{f, a, p\}$  denotes the trajectory group and  $Z_{i,t}^{(k)} = [z_1^{(k)}, \dots, z_{N^{(k)}}^{(k)}] \in \mathbb{R}^{N^{(k)} \times 320}$  is the resulting representation. According to Figure 4, the trajectory representation encoder is placed at the beginning of the trajectory processing pipeline. Importantly, its weights are frozen throughout the training pipeline, meaning it does not participate in backpropagation. This design choice allows us to pre-encode the trajectories into their instance-level representations  $Z_{i,t}^{(k)}$  prior to training. Doing so, we significantly improve memory efficiency, as we avoid training a highly memory-intensive nested transformer architecture, where long time-series sequences are first encoded into fixed-size vectors and then further embedded into a language-style sequence model. In contrast, pre-encoding the trajectories enables more efficient training without compromising the ability to incorporate rich temporal trajectory information.

#### 3.3.3. Cross-modality Adaptation Network

To enable integration between language-based prompt embeddings and trajectory-based time-series representations, we employ a cross-modality adaptation network, denoted as  $f_{\rm xa}(\cdot)$ , which adapts the trajectory inputs from

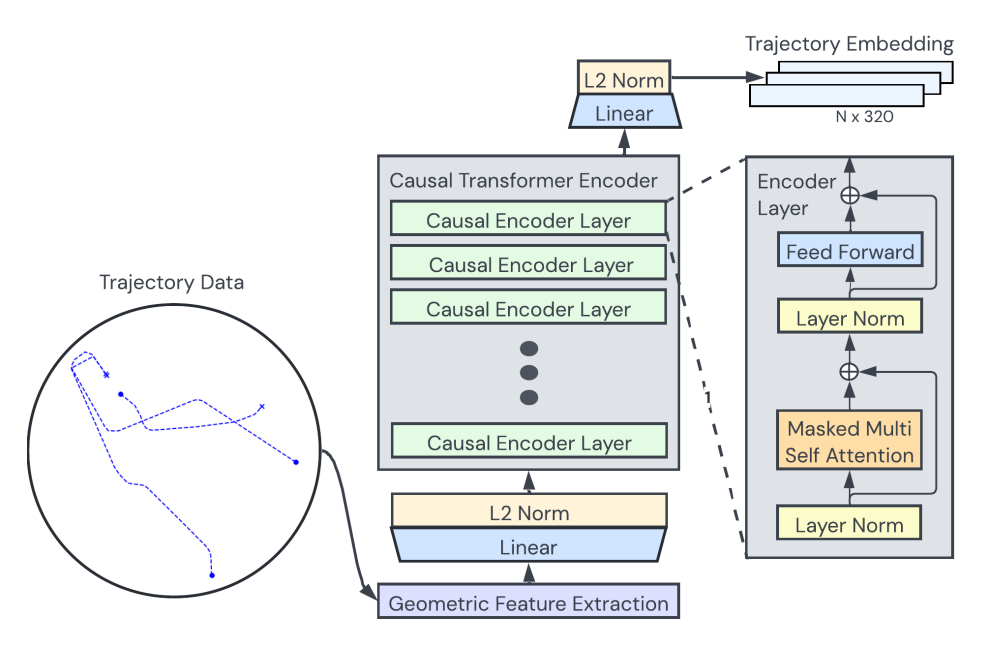


Figure 5: Architecture of Causal Transformer Encoder Trained with ATSCC

the time-series modality into the language modality. This network is structured as a lightweight MLP, designed to project instance-level trajectory representations into the language model's embedding space. Specifically, given the output from the pretrained trajectory encoder  $Z_{i,t}^{(k)} \in \mathbb{R}^{N^{(k)} \times 320}$ , the adaptation network transforms this vector into the LLM-friendly dimension d as follows:

$$\mathbf{Z}_{i,t}^{(k)} = f_{xa}(\mathbf{Z}_{i,t}^{(k)}),\tag{19}$$

where  $\mathbf{Z}_{i,t}^{(k)} \in \mathbb{R}^{N^{(k)} \times d}$  is the LLM-compatible embedding of trajectory group  $k \in \{f, a, p\}$  (focusing, active, or prior). The MLP architecture, which projects the 320-dimensional trajectory embedding to the LLM's model dimension of  $f_{xa}(\cdot)$ , comprises two linear layers with GELU activation functions and a dropout rate of 0.35 applied after each activation. The cross-modality adaptation network is simple and efficient, introducing only a small computational cost while effectively bridging the gap between trajectory encoders and LLMs. Its ability to integrate with the LLM without architectural changes highlights the practicality of cross-modal integration with minimal engineering effort. The embeddings  $\mathbf{Z}_{i,t}^{(k)}$  are inserted into designated positions within the tokenized static trajectory prompts, forming a unified input sequence of language and trajectory information processed by the LLM backbone. To combine the trajectories with textual embeddings, we insert trajectory embeddings between guiding prompts (Figure 12) to help the model distinguish different trajectory groups. The trajectory input is formally defined as:

$$\mathbf{Z}_{i,t}^{T} = \text{Concat}(\text{Emb}[T(P_{st,1})], \ \mathbf{Z}_{i,t}^{f}, \ \text{Emb}[T(P_{st,2})], \ \mathbf{Z}_{i,t}^{a}, \ \text{Emb}[T(P_{st,3})], \ \mathbf{Z}_{i,t}^{p}, \ \text{Emb}[T(P_{st,4})]), \tag{20}$$

This concatenated sequence  $\mathbf{Z}_{i,t}^T \in \mathbb{R}^{(L_{st,1}+1+L_{st,2}+N^a+L_{st,3}+N^p+L_{st,4})\times d}$  represents the complete trajectory-informed input for the multimodal model, where  $L_{st,k}$  denotes the length of the k-th static prompt segment after tokenization and embedding,  $1, N^a$ , and  $N^p$  are added to the embedding sequence length, as we use the instance-level representation of each trajectory as a single token.

#### 3.3.4. Large Language Model Backbone

To leverage pretrained linguistic understanding, we retain the LLM backbone while replacing its language modeling head with a regression head, enabling prediction of continuous post-terminal duration values. In this paper, we consider LLMs with sizes under 1.5 billion parameters, as the task is formulated as a single-value regression problem and does not require large-scale generative capacity. These small LLMs can run efficiently on a single consumer-grade GPU, demonstrating their suitability for deployment by a wider range of users. The candidate backbone models

include LLaMA3.2-1B, LLaMA3.2-1B-Instruct, Qwen2.5-1.5B, Qwen2.5-1.5B-Instruct, DeepSeek-R1-Distill-Qwen-1.5B, TinyLlama-v1.1, TinyLlama-1.1B-Chat-v1.0, and Pythia-1B. All model parameters and the embedding table are kept frozen as provided by the original sources to preserve their pretrained linguistic capabilities and ensure memory efficiency.

The LLM backbone processes multimodal inputs consisting of textual prompt embeddings,  $\mathbf{Z}_{i,t}^{p}$  obtained via the corresponding tokenizer and embedding table, and trajectory-informed embeddings  $\mathbf{Z}_{i,t}^{T}$  generated by the representation and cross-modality networks. Therefore, the input sequence fed to the LLM backbone is formed by concatenating these two components:

$$\mathbf{Z}_{i,t} = \operatorname{Concat}(\mathbf{Z}_{i,t}^p, \mathbf{Z}_{i,t}^T), \tag{21}$$

The concatenated sequence  $\mathbf{Z}_{i,t}$  is then passed through the LLM backbone:

$$\mathbf{h}_{i,t} = f_{\text{llm}}(\mathbf{Z}_{i,t})[-1],\tag{22}$$

and due to the autoregressive nature of causal language models, we extract only the last hidden state as the representation that summarizes all preceding tokens:  $\mathbf{h}_{i,t} \in \mathbb{R}^d$ , which is then used by the output regression head.

#### 3.3.5. Output Regression Head

For the final regression output, we attach a lightweight MLP output head to the model, which maps the final contextual representation  $\mathbf{h}_{i,t}$  to a scalar prediction. This vector  $\mathbf{h}_{i,t} \in \mathbb{R}^d$  is a multimodal encoding of the scenario  $s_{i,t}$ , capturing fused semantics from flight information, weather information, NOTAMs, and trajectory data. The regression head comprises three linear layers: the first maintains the LLM hidden size, the second halves the dimensionality, and the third outputs a scalar prediction. Each of the first two layers is followed by GELU activation and a 0.3 dropout rate. Formally, the model output is expressed as:

$$\hat{y}_i = f_h(\mathbf{h}_{i,t}),\tag{23}$$

where  $f_h(\cdot)$  denotes the MLP-based output head. This head allows the pretrained LLM backbone to be repurposed for regression tasks, efficiently producing a prediction from the rich multimodal context encoded in  $\mathbf{h}_{i,t}$ .

#### 3.4. Training Pipeline

For each scenario  $s_{i,t}$ , the textual components, general flight information, weather reports, and NOTAMs, are tokenized and embedded to form the prompt embedding  $\mathbf{Z}_{i,t}^p$ . Separately, the static prompts that describe the structure and semantics of the trajectory groups (focusing, active, and prior) are combined with their corresponding instance-level representations, which were pre-encoded by the frozen ATSCC model  $f_{\text{atscc}}$  and projected via the trainable adapter  $f_{\text{xa}}$  to form the trajectory-informed sequence  $\mathbf{Z}_{i,t}^T$ . Those embedding sequences are concatenated into a unified sequence  $\mathbf{Z}_{i,t}$ , which is then fed into the frozen LLM backbone  $f_{\text{llm}}$ . Since the LLM is a causal model, only the final hidden state  $\mathbf{h}_{i,t}$  is extracted, representing a context-aware summary of the entire input sequence. This hidden state is passed to a trainable regression head  $f_h$  to produce a scalar prediction  $\hat{y}_i$ , corresponding to the estimated time spent in the airspace. The ground-truth target  $y_i$  is standardized prior to training. Optimization is performed using the AdamW optimizer with a learning rate of  $1 \times 10^{-5}$ , weight decay of  $1 \times 10^{-5}$ , and a mini-batch size of 4. The model is trained using the Smooth L1 Loss:

$$\mathcal{L}_{\text{smooth}}(\hat{y}, y) = \begin{cases} 0.5 \cdot (\hat{y} - y)^2, & \text{if } |\hat{y} - y| < 1\\ |\hat{y} - y| - 0.5, & \text{otherwise} \end{cases}$$
 (24)

which is robust to outliers, well-suited, and in some cases, prevents exploding gradients [84]. The parameters of the pretrained components, namely the embedding table Emb, LLM backbone  $f_{\rm llm}$ , and the trajectory encoder  $f_{\rm atscc}$ , are frozen. Only the cross-modality adaptation network  $f_{\rm xa}$  and the regression head  $f_h$  are updated during training, as illustrated in Figure 4, ensuring memory efficiency by avoiding gradient allocation to the LLM and trajectory models. All training and evaluation are conducted using Python 3.11.8 and PyTorch 2.0.1 with CUDA Toolkit 11.8, running on an NVIDIA GeForce RTX 4090 GPU.

# Algorithm 1 Multimodal Training Pipeline for Flight Delay Regression

```
1: Input: Scenario dataset S = \{(s_{i,t}, y_i)\}_{i=1}^N, where s_{i,t} = \{P_{i,t}^{fp}, P_t^{wx}, P_t^{no}, X_{i,t}^f, X_{i,t}^a, X_{i,t}^p\}
 2: Output: Trained model parameter \theta
 3: for s_{i,t} in S do
             Z_{i,t}^{(j)} = f_{\text{atscc}}(X_{i,t}^{(j)}), \quad j \in \{f, a, p\}
  5: end for
 6: for each epoch do
            for each batch \mathcal{B} \subset \mathcal{S} do
 7:
 8:
                  for each scenario (s_{i,t}, y_i) in \mathcal{B} do
                        Build prompt P_{i,t} = P_{i,t}^{fp} \parallel P_t^{wx} \parallel P_t^{no}
\mathbf{Z}_{i,t}^p = \operatorname{Emb}[T(P_{i,t})]
 9:
10:
                        \mathbf{Z}_{i,t}^{(j)} = f_{xa}(Z_{i,t}^{(j)}), \quad j \in \{f, a, p\}
11:
                        \mathbf{Z}_{i,t}^{T} = \text{Concat}(\text{Emb}[T(P_{st,1})], \ \mathbf{Z}_{i,t}^{f}, \ \text{Emb}[T(P_{st,2})], \ \mathbf{Z}_{i,t}^{a}, \ \text{Emb}[T(P_{st,3})], \ \mathbf{Z}_{i,t}^{p}, \ \text{Emb}[T(P_{st,4})])
12:
                        \mathbf{Z}_{i,t} = \text{Concat}(\mathbf{Z}_{i,t}^p, \mathbf{Z}_{i,t}^T)
13:
                        \mathbf{h}_{i,t} = f_{\text{llm}}(\mathbf{Z}_{i,t})[-1]
14:
                        \hat{\mathbf{y}}_i = f_h(\mathbf{h}_{i,t})
15:
16:
                  \mathcal{L} = \frac{1}{|\mathcal{B}|} \sum_{i} \text{SmoothL1Loss}(\hat{y}_i, y_i)
17:
                   Backpropagate and update trainable parameters in f_{xa}(\cdot) and f_{b}(\cdot)
18:
19:
20: end for
```

#### 4. Results and Discussion

This section begins by outlining the evaluation metrics used to assess the model after updating the parameters of the cross-modality adaptation network  $f_{xa}(\cdot)$  and the regression head  $f_h(\cdot)$ . We then compare model performance across different LLM backbones to examine how linguistic capability affects prediction accuracy. Finally, we conduct a prompt structure analysis to evaluate the importance of each type of aeronautical information and its contribution to delay prediction accuracy.

#### 4.1. Evaluation Metrics

To quantify the model's predictive accuracy, we first evaluate its ability to predict the post-terminal duration  $y_i \equiv \Delta t_{post,i}$  directly from the scenario input  $s_{i,t}$ , formulated as  $\hat{y}_i = f_{\theta}(s_{i,t})$ . Ultimately, we assess the model's effectiveness in estimating the total delay  $D_i$ , by incorporating the known actual entry time  $T_{entry,i}^{act}$  and scheduled arrival time  $T_{arr,i}^{sch}$ , expressed as  $\hat{D}_i = \left(T_{entry,i}^{sch} - T_{arr,i}^{sch}\right) + \hat{y}_i$ . The performance of both predictions is evaluated using a set of standard regression metrics. These metrics collectively capture various aspects of model performance, including the average magnitude of prediction errors, their squared severity, relative error scaling, and the proportion of variance explained by the model.

• Mean Absolute Error (MAE) measures the average magnitude of errors in predictions, without considering their direction. The evaluation on total delay is given by:

$$MAE = \frac{1}{N} \sum_{i=1}^{N} \left| \hat{D}_i - D_i \right|$$
 (25)

$$= \frac{1}{N} \sum_{i=1}^{N} \left| \left( T_{entry}^{act} - T_{arr}^{sch} + \hat{y}_i \right) - \left( T_{entry}^{act} - T_{arr}^{sch} + y_i \right) \right|$$
 (26)

$$= \frac{1}{N} \sum_{i=1}^{N} |\hat{y}_i - y_i| \tag{27}$$

Therefore, the evaluation on the total delay is equivalent to evaluating the prediction of the post-terminal duration. MAE is easy to interpret and robust to outliers, as it represents the average magnitude of errors in absolute terms. However, it may not adequately reflect the impact of larger errors due to its linear penalty formulation.

• Mean Squared Error (MSE) squares each error term, thus giving more weight to larger errors. The MSE evaluation on the delay is calculated by:

$$MSE = \frac{1}{N} \sum_{i=1}^{N} (\hat{D}_i - D_i)^2$$
 (28)

$$= \frac{1}{N} \sum_{i=1}^{N} \left( \left( T_{entry}^{act} - T_{arr}^{sch} + \hat{y}_i \right) - \left( T_{entry}^{act} - T_{arr}^{sch} + y_i \right) \right)^2$$
 (29)

$$= \frac{1}{N} \sum_{i=1}^{N} (\hat{y}_i - y_i)^2 \tag{30}$$

Thus, similar to MAE, the calculation of MSE for the total delay yields the same result as that for the post-terminal duration. MSE is particularly sensitive to outliers due to its quadratic error term, making it well-suited for scenarios where larger deviations from the actual values are especially critical.

• Root Mean Squared Error (RMSE) is the square root of MSE:

$$RMSE = \sqrt{MSE}$$
 (31)

RMSE combines the benefits of MSE's sensitivity to large errors with a more intuitive scale for assessment.

• Symmetric Mean Absolute Percentage Error (SMAPE) measures the relative prediction error as a percentage. The SMAPE for delay prediction and post-terminal duration prediction is given as follows:

$$SMAPE_{D} = \frac{100\%}{N} \sum_{i=1}^{N} \frac{\left| \hat{D}_{i} - D_{i} \right|}{\left( \left| D_{i} \right| + \left| \hat{D}_{i} \right| \right) / 2}$$
(32)

$$SMAPE_{\Delta t} = \frac{100\%}{N} \sum_{i=1}^{N} \frac{|\hat{y}_i - y_i|}{(|y_i| + |\hat{y}_i|)/2}$$
(33)

Due to the absolute terms in SMAPE's denominator, we separately evaluate delay prediction (SMAPE<sub>D</sub>) and post-terminal duration prediction (SMAPE<sub> $\Delta t$ </sub>). SMAPE is used instead of MAPE to reduce instability from zero ground truth values, common in on-time flights. While SMAPE can still be unstable when true or predicted values are near zero, it is generally more robust than MAPE.

• Coefficient of Determination ( $R^2$ ) quantifies the proportion of variance in the dependent variable explained by the model. The  $R^2$  scores for both delay and post-terminal duration prediction are computed as follows:

$$R_D^2 = 1 - \frac{\sum_{i=1}^{N} (\hat{D}_i - D_i)^2}{\sum_{i=1}^{N} (D_i - \bar{D})^2}$$
(34)

$$R_{\Delta t}^2 = 1 - \frac{\sum_{i=1}^{N} (\hat{y}_i - y_i)^2}{\sum_{i=1}^{N} (y_i - \bar{y})^2}$$
(35)

Due to the presence of the mean in the denominator, the  $R^2$  score for total delay  $(R_D^2)$  cannot be equivalent to that of the post-terminal duration  $(R_{\Delta t}^2)$ ; thus, they are evaluated separately. The  $R^2$  score provides an intuitive measure of goodness-of-fit, indicating the proportion of variance explained by the model. While it can be misleading for small or imbalanced datasets, this is less of a concern given the scale and diversity of our data.

#### 4.2. Model Performance

This section illustrates the performance of our framework when integrated with various LLM backbones, allowing for a direct comparison of how the varying linguistic capabilities of pre-trained LLMs with different architectures

 Table 3

 Average Model Performance Comparison

LLM Backbone	MAE↓	MSE↓	RMSE↓	$SMAPE_D^{\perp}$	$R_{\scriptscriptstyle D}^2{}^{\uparrow}$	$SMAPE_{\Delta t}^{\downarrow}$	$R^2_{\Delta t}$ $^{\uparrow}$
LLaMA3.2-1B	0.9911	2.2794	1.5036	11.3009	0.99980	7.9400	0.9134
LLaMA3.2-1B-Instruct	0.9214	1.9965	1.4111	10.6924	0.99982	7.1308	0.9244
Qwen2.5-1.5B	1.1840	3.2651	1.7989	12.8570	0.99971	9.0699	0.8763
Qwen2.5-1.5B-Instruct	1.1970	3.4163	1.8335	13.0869	0.99969	9.1841	0.8705
DeepSeek-R1-Distill-1.5B	1.0469	2.5713	1.6000	11.7409	0.99977	7.8834	0.9026
TinyLlama-v1.1	1.0268	2.4719	1.5684	11.5998	0.99978	7.9976	0.9059
TinyLlama-1.1B-Chat-v1.0	0.9988	2.3257	1.5192	11.3519	0.99980	7.8986	0.9117
Pythia-1B	0.9551	2.1284	1.4545	11.0689	0.99981	7.4839	0.9192

<sup>↓</sup> Lower is better, ↑ Higher is better.

and training strategies impact prediction accuracy. Our evaluation protocol trains the overall model while replacing the LLM backbone with various candidates. For each backbone, we conduct experiments on 12 monthly datasets from 2022, training and testing separately on each month's corresponding train-test split, visualized in Figure 3. Each scenario  $s_{i,t}$  contains the full context, including flight plan, weather, NOTAMs, and trajectories representing airspace conditions. This full context is provided to the model to indirectly predict the total delay  $D_i$  through the estimation of the post-terminal duration  $\hat{y}_i = f_{\theta}(s_{i,t})$ , using hyperparameters strictly following the reproduction details.

Table 3 presents a performance comparison of several lightweight LLMs on the flight delay prediction task. Among the models evaluated, LLaMA-3.2-1B-Instruct consistently outperforms others across all key metrics for many months. We hypothesize that its high-quality pretraining corpus contributes to its ability to generalize to aeronautical information. Its instruction-tuned training enhances the ability to follow structured prompts, and despite having relatively few parameters, it remains capable of capturing long context in post-terminal duration prediction.

Across the evaluated models, those trained primarily as English single-language models, unlike the Qwen-based model, tend to outperform multilingual models, suggesting that linguistic alignment with the structured English prompts in our framework provides an advantage. Interestingly, DeepSeek-R1-Distill-Qwen-1.5B, although distilled from the math-specialized Qwen-2.5-1.5B-Math model, performs better than its Qwen counterparts, suggesting that the distillation process may have introduced useful generalization capabilities. The TinyLLaMA variants demonstrate competitive performance, although they generally do not achieve the accuracy of LLaMA-3.2 models. In addition, the Pythia-1B model achieves strong results, in some cases exceeding LLaMA-3.2-1B-Instruct, suggesting that it can be a suitable candidate under appropriate training conditions.

Although all models are provided with the full context and trained until the trajectory embeddings align with the tokens that enable the LLM to predict delays with minimal error, different LLM backbones still exhibit varying levels of performance. This reflects the importance of the models' linguistic understanding in achieving accurate post-terminal duration prediction. Thus, it is not only the inclusion of the full context that matters, but also the model's ability to effectively interpret that context in order to achieve the best prediction results.

In addition to assessing the comparative effectiveness of each model, we demonstrate that our proposed framework is compatible with arbitrary LLM backbones, as it consistently integrates trajectory representations with the language modality for accurate delay prediction across different models. This highlights the potential of the proposed cross-modality adaptation technique for application to larger and more capable models.

Our framework achieves high  $R_D^2$  values due to our unique problem formulation, which leverages information already available to ATCs at the destination aerodrome, namely, the scheduled time of arrival and the actual time when the aircraft enters the TMA, marking the start of monitoring. This enables efficient prediction without the need for historical delay data or airport network information, unlike the sequential and graph-based models compared in Table 1. By narrowing the focus to a single airport, the framework aligns with the operational scope of ATCs and achieves significantly more accurate delay prediction, without requiring the ability to monitor many airports simultaneously.

From a practical perspective, our framework with several backbones maintains prediction error within one minute and can be considered deployable, as delays are typically recorded at the minute level [75]. While second-level accuracy may be desirable for certain operational needs, the framework already meets the current standard of minute-level records, and future access to higher-resolution data could provide opportunities for even greater precision.

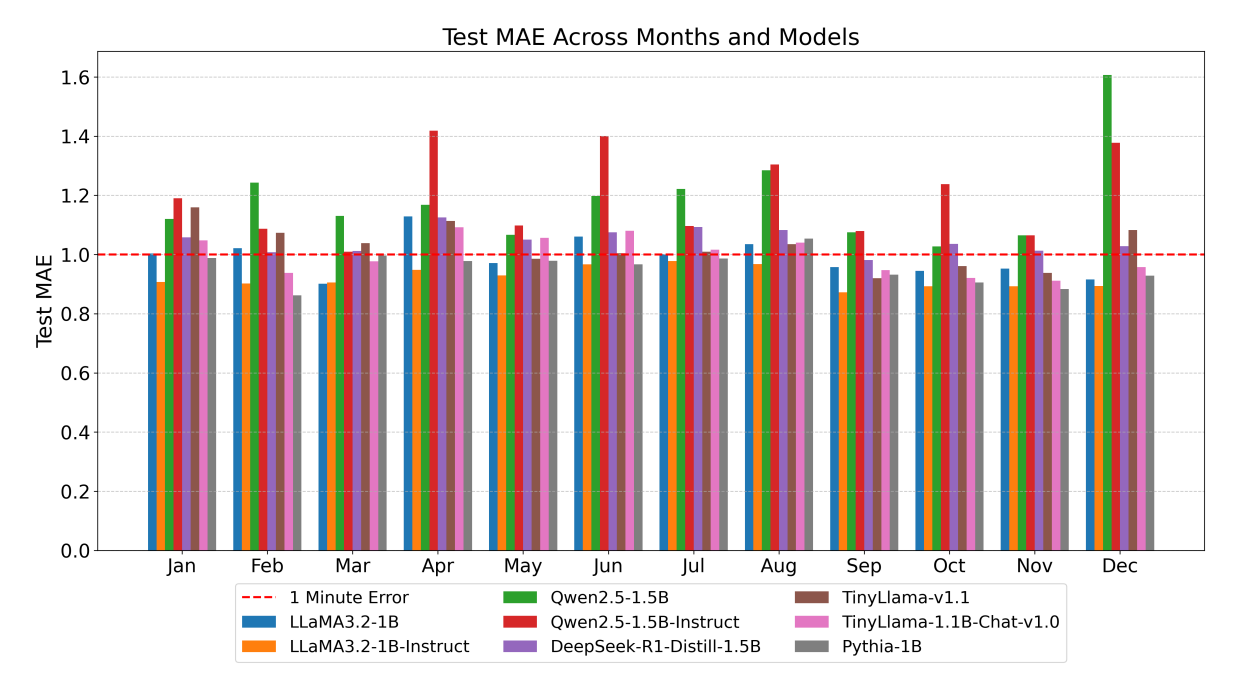


Figure 6: Test MAE Across Months and Models

#### 4.3. Effectiveness of Context Inclusion

A key contribution of our proposed framework is the integration of a comprehensive set of information, providing a representation of the operational environment to the model, including general flight information, weather reports and forecasts, NOTAMs, and airspace conditions modeled through three types of trajectories set. These contextual components are of varying importance; therefore, to evaluate their contributions, we adopt an ablation-based approach in which each component is selectively removed from the multimodal scenario representation  $s_{i,t}$ , followed by retraining and re-evaluation under strictly identical hyperparameter settings. We used Meta's LLaMA-3.2-1B-Instruct as the LLM backbone, for the results presented in Table 3 show that the model consistently outperforms other LLMs across the majority of datasets and evaluation metrics. This controlled procedure enables us to directly quantify the performance degradation resulting from the absence of each context type, thereby providing empirical evidence for its contribution to the overall predictive capability. Moreover, this analysis was conducted to support our design choice of using full context in the final configuration, demonstrating the value of leveraging multimodal aeronautical data for accurate prediction of  $\Delta t_{nost}$ . The importances of context elements are discussed as follows:

- **Texual Data:** Since the textual data provides the context for flight information, weather, and NOTAMs, removing them consistently degrades performance. This indicates that the LLM relies on textual context in addition to trajectory features for prediction. While the trajectory is directly proportional to the post-terminal duration, the extension of this duration is strongly influenced by the surrounding operational context.
- General Flight Information: The exclusion of basic flight information leads to a clear drop in performance, underscoring the importance of general operation details of the flight. This finding aligns with prior works, which predominantly rely on general flight information as the primary input for delay prediction, as shown in Table 1.
- Weather Information: The exclusion of weather information, including both METAR and TAF reports, leads to a decrease in model performance. This observation is consistent with many prior studies that weather data is a critical input for delay prediction (Table 1). It also aligns with the analysis in [3], which identifies weather as a major factor contributing to flight delays and emphasizes its necessity as context for accurate prediction.
  - METAR Information Removing METAR while keeping TAF makes the model depend solely on forecasts. Having at least TAF still enables the model to perform better than removing all weather information,

- since TAF, when recently issued and accurate, can also approximate current weather conditions. However, without METAR, which provides real-time weather observation, the model's performance slightly drops.
- TAF Information We observe that removing TAF while retaining METAR can, in some months, improve performance, likely due to the reduced burden of long contextual inputs. However, on average, the absence of TAF leads to a larger performance drop than removing METAR, indicating that forecast information still contributes valuable signals for delay prediction beyond real-time observations.
- NOTAMs: Excluding NOTAMs shortens the contextual input, which can sometimes reduce the burden of long sequences. However, it also removes special operational constraints or disruptions, such as runway closures or equipment failures, which can introduce sources of delay [3]. As a result, performance is noticeably reduced overall. This supports our design choice of incorporating NOTAMs as input for post-terminal duration prediction, thereby improving delay estimation.
- **Trajectory Data:** Trajectory data is shown to be the most influential factor for post-terminal duration prediction, as its exclusion results in a severe reduction in performance. This is expected, since trajectory data inherently reflect real-time airspace awareness that cannot be inferred from static flight or weather information alone. From a technical perspective, removing trajectory inputs also eliminates the learnable portion of the model's context. This suggests that integrating trajectory data contributes to the predictive accuracy of our framework.
  - Focusing Trajectories We find that removing the focusing trajectory leads to a large performance degradation, often comparable to the removal of all trajectory inputs and consistently more severe than excluding other trajectory types. This finding is expected and aligns with [25], as the focusing trajectory embedding captures the specific maneuvering procedures being executed and the state of the current flight under monitoring, which are most directly related to its post-terminal duration.
  - Active Trajectories Excluding the active trajectories from the combined input removes the model's
    awareness of the current airspace conditions, particularly the level of traffic congestion and the overall
    traffic situation at that time. Therefore, the model cannot account for the congestion factor that often extends
    the post-terminal duration, making accurate prediction more difficult.
  - Prior Trajectories Since prior trajectories provide patterns that may influence the active and focusing
    trajectories and indirectly reflect ground traffic, excluding them leaves the model unaware of historical
    flow patterns in both air and ground operations, thereby reducing predictive accuracy.

The experimental results indicate that our accurate predictions are enabled by offering a different formulation from prior works and by incorporating more contextual information within a single airspace, as compared in Table 1. While long contextual inputs can sometimes cause the model to struggle, removing certain elements, such as TAFs and NOTAMs, from many datasets may even improve performance. However, including the full context generally ensures consistent and reliable results, as the model can rely on that information when it is actually required. Since LLMs function as selective sequence encoders with the ability to disregard irrelevant tokens, it is preferable to provide the full context and allow the model to ignore unneeded tokens rather than risk excluding potentially useful information.

The contribution of textual components follows a similar pattern, though the trajectory components play a more critical role. This is partly because trajectory features are trainable and partly because the post-terminal duration is strongly influenced by prevailing traffic conditions. Moreover, durations in other phases of flight are implicitly accounted for through events that occur during the pre-terminal phases. The framework demonstrates robustness even when certain contextual information is unavailable, underscoring its suitability for operational use. Without such a model, air traffic controllers would need to assume an average additional more than 3 minutes for every flight [85], which could introduce unnecessary errors for non-delayed aircraft. In contrast, our model achieves an average error between 0.9214 and 2.7395 minutes, highlighting its accuracy and operational value.

#### 4.4. Demonstration for Second-by-Second Delay Update

From the perspective of an ATC, delay information should be updated in real time. Unlike prior works, where delay is typically predicted at a coarse time scale, constrained by the low update frequency of input contexts such as weather data (e.g., every 30 minutes), our framework can provide second-level monitoring because it incorporates surveillance broadcast signals, which are transmitted frequently and thus allow the context to be updated in real time. In this section,

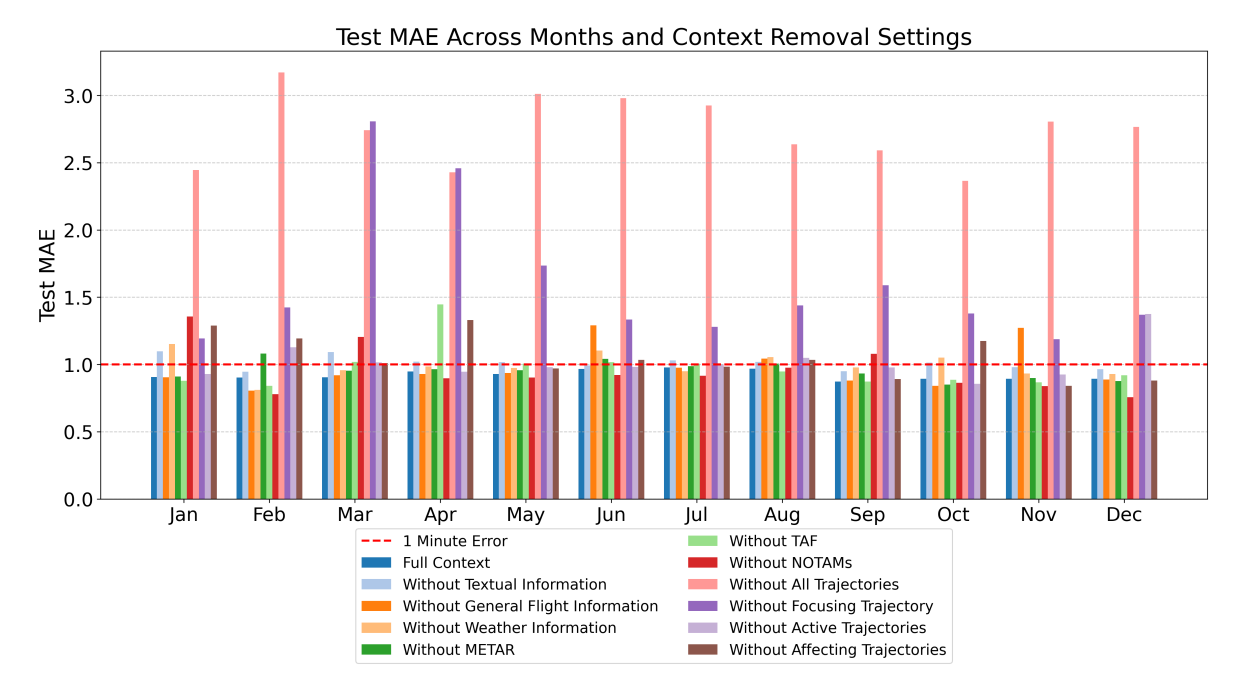


Figure 7: Test MAE Across Months and Context Removal Settings

Table 4
Prompt Component Ablation Results using Meta-LLaMA-3.2-1B-Instruct

Ablation Tag	MAE↓	MSE↓	RMSE↓	$SMAPE_D^{\downarrow}$	$R_D^2$ $^{\uparrow}$	$SMAPE_{\Delta t}^{\downarrow}$	$R^2_{\Delta t}$ $^{\uparrow}$
Full Context	0.9214	1.9965	1.4111	10.6924	0.99982	7.1308	0.9244
Without Textual Information	1.0103	2.3610	1.5331	11.4995	0.99979	7.8583	0.9105
Without Flight Information	0.9738	2.2846	1.4955	11.1673	0.99979	7.8250	0.9142
Without Weather Information	0.9898	2.3286	1.5153	11.3504	0.99979	7.6066	0.9119
Without METAR	0.9549	2.1245	1.4534	11.0112	0.99981	7.3700	0.9197
Without TAF	0.9757	2.2584	1.4855	11.0981	0.99981	7.6145	0.9131
Without NOTAMs	0.9573	2.1403	1.4428	10.8942	0.99982	7.5266	0.9188
Without All Trajectories	2.7395	16.3961	4.0383	23.3048	0.99852	22.4923	0.3826
Without Focusing Trajectory	1.5997	6.7335	2.4641	15.6197	0.99944	14.2710	0.7387
Without Active Trajectories	1.0137	2.3863	1.5368	11.6211	0.99979	7.9227	0.9098
Without Prior Trajectories	1.0528	2.6147	1.6005	11.8261	0.99977	8.3614	0.9001

<sup>↓</sup> Lower is better, ↑ Higher is better.

we demonstrate the real-time capability of our model by using a network trained on January data and testing it on a sample trajectory from February. For each second along this trajectory, we construct a textual prompt that includes general flight information, weather reports, and NOTAMs, and we retrieve the corresponding focusing, active, and prior trajectories of the flight at that time. This setting challenges the model with entirely unseen data and evaluates its ability to provide continuous predictions. The selected trajectory, along with the prediction results and absolute errors over the terminal phase time horizon, is visualized in Figure 8.

Although the model underestimates the delay in this example, we observe that the absolute error generally remains within one minute, with predictions adapting as the flight progresses. Moreover, the variation in error over time suggests that the model refines its predictions as newly available information updates the prediction context. Importantly, maintaining sub-minute error levels is practically useful for ATM, since delays are typically recorded at the minute level [75]; keeping the error below one minute is therefore considered deployable. Thus, the real-time prediction model

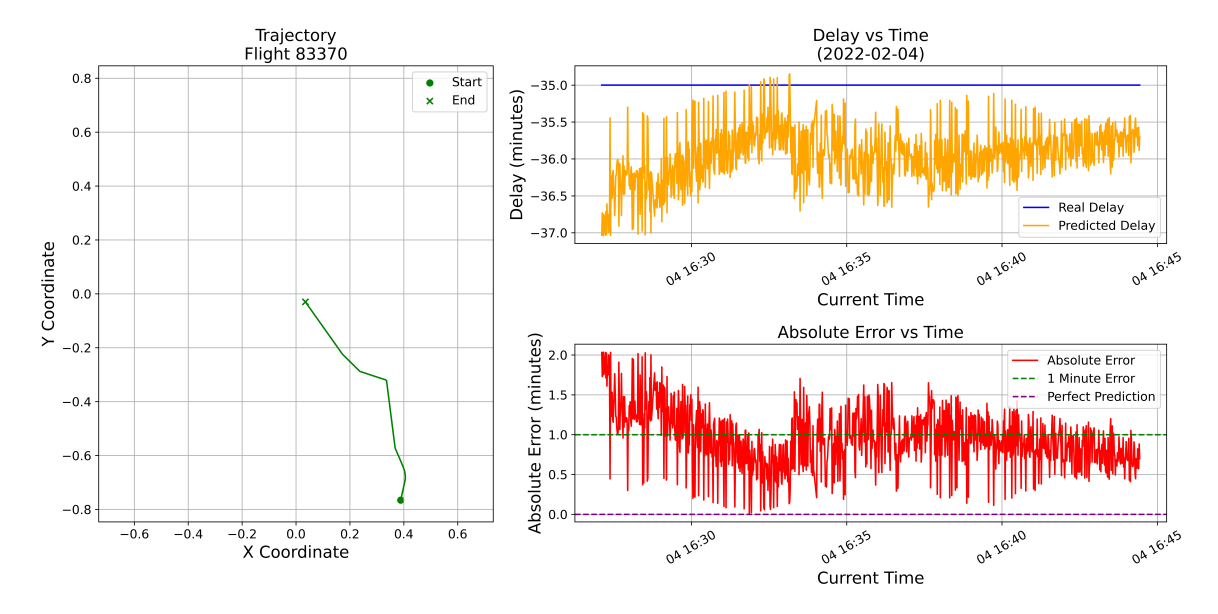


**Figure 8:** Demonstration of Second-by-Second Delay Updates. Left: Full trajectory; top-right: predicted delay versus actual delay; bottom-right: absolute error over time.

from our framework can potentially be integrated into post-terminal ATM systems to assist ATCs in estimating the delay of aircraft within the terminal area.

## 5. Conclusion

This paper presents a flight delay prediction framework that indirectly estimates post-terminal delays by predicting post-terminal duration. Since flight schedules and airspace entry times are already known to ATCs at the destination airport, the framework is designed to support their operational needs by providing accurate and continuously updated delay information. It employs a cross-modality adaptation technique that aligns multimodal data with LLMs, adapting trajectory embeddings from a pre-trained ATSCC encoder into the language modality. The training process remains lightweight, leveraging the pretrained knowledge of both the trajectory encoder and the LLM, while only updating a cross-modality adaptation network and an output regression head for prediction. The framework enables accurate post-terminal duration prediction, with performance gains driven by the comprehensive inclusion of aeronautical information, especially trajectory data, which contribute the most after the cross-modality adaptation. These inputs allow the model to reference key factors influencing delays, while the linguistic capabilities of LLMs enable the interpretation of complex contextual information. By incorporating a wide range of context within the narrower airspace setting, our framework addresses several key limitations of prior works, such as the reliance on prior delay information, the requirement for structured inputs, and the restriction to coarse update timescales. In contrast, our approach focuses on the real-time situation in the airspace, incorporates prior delays through information already available to ATC, flexibly integrates all necessary context, and supports second-by-second updates, making it particularly well-suited for real-time post-terminal ATM operations. Looking forward, the framework can be extended to other phases of delay prediction by incorporating contextual factors relevant to those phases. Furthermore, its generality opens opportunities for broader ATM tasks, such as trajectory prediction and conflict detection. Future work may also explore the integration of higher-quality operational data and additional modalities, such as images or audio, to further advance multimodal models in aviation research in a practical and easily deployable manner.

# A. Prompt Structure

# A.1. General Flight Information Prompt

From the general flight information, which includes multiple data types as described in Table 2, we convert the data into a format compatible with language models using 10 distinct prompt templates. Examples of these prompt formats are illustrated in Figure 9. These templates convert structured data into natural language, aligning better with LLM pretraining knowledge. Moreover, using multiple formats improves prompt generalization of the trainable components by training the model with varied expressions of the same content.

# General Flight Information Prompt Format Example

Scheduled for arrival at {sched\_time\_utc} UTC on {date} ({day\_of\_week}), flight {callsign\_code\_iata}/{callsign\_code\_icao} by {airline\_name\_english} was set to land at {dest\_name\_english} ({dest\_code\_iata}/{dest\_code\_icao}, lat: {dest\_lat}, lon: {dest\_lon}, alt: {des\_altitude} ft). The aircraft originated from {dep\_name\_english} ({dep\_code\_iata}/{dep\_code\_icao}, lat: {dep\_lat}, lon: {dep\_lon}, alt: {dep\_altitude} ft), and the total route spanned {distance} km. The aircraft was a {aircraft\_type} with registration {aircraft\_registration}, and it belonged to the {wake\_turbulence\_cat} wake turbulence category. It was expected to enter airspace or appear via ADS-B at {actual\_entry\_time}. This was a {haul}-haul flight.

#### General Flight Information Prompt Format Example

On {date}, a {haul}-haul flight by {airline\_name\_english} was scheduled to arrive at {dest\_name\_english} ({dest\_code\_icao}/{dest\_code\_iata}) at {sched\_time\_utc} UTC. Flight ID: {callsign\_code\_icao}/{callsign\_code\_iata}. The aircraft departed from {dep\_name\_english} ({dep\_code\_icao}, lat: {dep\_lat}, lon: {dep\_lon}, alt: {dep\_altitude} ft) and was destined for {dest\_name\_english}, located at lat: {dest\_lat}, lon: {dest\_lon}, alt: {dest\_altitude} ft. The aircraft was a {aircraft\_type} with registration {aircraft\_registration}, and it belonged to the {wake\_turbulence\_cat} wake turbulence category. The aircraft was expected to enter monitored airspace around {actual\_entry\_time}. Day of week: {day\_of\_week}, distance: {distance} km.

Figure 9: Examples of Prompt Format for General Flight Information Description

#### **A.2.** Weather Prompt

The weather prompt  $P_t^{wx}$  is constructed from the METAR and TAF data queried at time t retrieved during dataset preparation. These coded weather reports are parsed and reformatted into natural language prompts following a predefined structure. An example of the formatted weather prompt is shown in Figure 10.

#### Weather Information Prompt Format Example

METAR in effect: 202202272230 METAR RKSI 272230Z 14006KT 5000 BR NSC 01/M00 Q1023 NOSIG=
TAF in effect: 202202271700 TAF RKSI 271700Z 2718/2824 21006KT CAVOK TN01/2722Z TX08/2806Z
TN03/2820Z BECMG 2721/2722 14006KT 4000 BR NSC BECMG 2800/2801 21006KT 6000 NSW BECMG
2814/2815 14010KT BECMG 2817/2818 17006KT 3500 -RA FEW010 BKN025 OVC100 TEMPO 2822/2824
29006KT 0800 DZ FG BKN005

Figure 10: Example of Formatted Weather Information Prompt

## A.3. NOTAM Prompt

The NOTAM prompt  $P_t^{no}$  is constructed from all active NOTAMs at time t, capturing time-specific operational constraints. Instead of decoding aeronautical codes, we maintain the raw text and format it using a fixed template (Figure 11), similar to the weather information prompt.

#### Special Notices Prompt Format Example

Active NOTAMs: REF AIP SUP 31/22, A-CDM PHASE 2 TRIAL OPERATION PROGRESSIVE STEPS 2 AND 3 PERIOD CHG AS FLW 1. STEP 2: FROM 1600 UTC 29 JUN 2022 TO 1600 UTC 11 JAN 2023 2. STEP 3: FROM 1600 UTC 11 JAN 2023 TO 1600 UTC 27 JUN 2023) TEMP OBST(CRANES) ERECTED AS FLW 1. PSN: 372806.54N 1262700.83E, 372740.28N 1262724.18E 2. RADIUS: 10M 3. HGT: 20.24M(66.4FT) AMSL) TEMP OBST(CRANES) ERECTED AS FLW 1. PSN: 372812.81N 1262551.43E, 372815.70N 1262553.51E, 372814.91N 1262557.46E, 372812.15N 1262552.41E 2. RADIUS: 40M 3. HGT: 60.39M(198.13FT) AMSL) TDWR(TERMINAL DOPPLER WEATHER RADAR) U/S DUE TO WIP)

Figure 11: Example of Formatted Special Aerodrome Notices (NOTAMs) Prompt

# A.4. Static Guiding Prompt for Trajectories

Three types of trajectories,  $X_{i,t}^f$ ,  $X_{i,t}^a$ , and  $X_{i,t}^p$ , represent distinct aspects of the airspace situation surrounding the flight of interest. To help the model distinguish and reason over these inputs, we introduce a structured prompt that explicitly labels each trajectory group. The guiding prompt segments specify which input embeddings correspond to each trajectory type, thereby helping the model distinguish their distinct semantic roles.

```
Trajectory Prompt P_{st,1}: Focus Trajectory

Airspace is described using three trajectory types. This embedding is for the focus trajectory: {

Trajectory Prompt P_{st,2}: Active Trajectories

} These embeddings are for other active trajectories: {

Trajectory Prompt P_{st,3}: Prior Trajectories

} These embeddings are for past or inactive trajectories that may still matter:{

Trajectory Prompt P_{st,4}: Closing Prompt

} Missing types will have no embedding. Based on the above, predict the total time spent in the airspace.
```

Figure 12: Static Prompt Segments for Trajectory Type Descriptions within Scenario Prompts

The static prompts (Figure 12) will be tokenized and embedded in parallel with the trajectory embeddings obtained through a trajectory representation model and a cross-modality adaptation network. The instance-level representations of the trajectories are inserted between the static prompt segments, resulting in a unified language-time series embedding that describes the airspace. This design mirrors how human operators visualize dynamic traffic, thereby enabling effective modeling of airspace conditions without dependence on tasks such as traffic count, traffic classification, capacity assessment, or conflict detection.

# **B. Full Model Comparison Results**

**Table 5**Model Performance Metrics for Q1-Q2 (January–June)

Month	Model	MAE↓	MSE <sup>↓</sup>	RMSE↓	$SMAPE_{D}^{\downarrow}$	$R_D^2$ $^{\uparrow}$	$SMAPE_{\Delta t}^{\downarrow}$	$R_{\Delta t}^{2}$
	LLaMA3.2-1B	1.0037	2.4014	1.5497	8.4650	0.99990	8.3901	0.9048
	LLaMA3.2-1B-Instruct	0.9074	2.1798	1.4764	7.7226	0.99991	7.5289	0.9136
	Qwen2.5-1.5B	1.1204	3.0157	1.7366	9.3075	0.99987	9.0874	0.8805
lanuani	Qwen2.5-1.5B-Instruct	1.1903	3.2394	1.7998	10.0064	0.99986	9.9379	0.8716
January	DeepSeek-R1-Distill-1.5B	1.0579	2.7419	1.6559	8.8657	0.99988	8.4753	0.8913
	TinyLlama-v1.1	1.1592	3.2552	1.8042	9.4798	0.99986	9.7450	0.8710
	TinyLlama-1.1B-Chat-v1.0	1.0482	2.6411	1.6251	8.9892	0.99989	8.2527	0.8953
	Pythia-1B	0.9884	2.5769	1.6053	8.4581	0.99989	8.3523	0.8979
	LLaMA3.2-1B	1.0218	2.0502	1.4318	9.7268	0.99988	10.7475	0.9249
	LLaMA3.2-1B-Instruct	0.9023	1.7515	1.3234	8.6933	0.99990	8.3369	0.9358
	Qwen2.5-1.5B	1.2429	2.8620	1.6917	11.4294	0.99983	10.7699	0.8952
February	Qwen2.5-1.5B-Instruct	1.0868	2.3503	1.5331	10.4437	0.99986	9.5309	0.9139
rebruary	DeepSeek-R1-Distill-1.5B	1.0078	2.1312	1.4599	9.7570	0.99987	8.8340	0.9219
	TinyLlama-v1.1	1.0731	2.3178	1.5224	10.4845	0.99986	9.6429	0.9151
	TinyLlama-1.1B-Chat-v1.0	0.9382	1.7698	1.3303	9.2389	0.99990	9.1174	0.9352
	Pythia-1B	0.8619	1.5463	1.2435	8.6889	0.99991	8.0699	0.9434
	LLaMA3.2-1B	0.9014	1.5692	1.2527	8.6175	0.99989	7.3750	0.9410
	LLaMA3.2-1B-Instruct	0.9054	1.9429	1.3939	8.3270	0.99986	7.5979	0.9269
	Qwen2.5-1.5B	1.1308	2.9306	1.7119	10.0066	0.99979	9.0807	0.8898
March	Qwen2.5-1.5B-Instruct	1.0091	2.3622	1.5369	9.2749	0.99983	8.3688	0.9112
iviaicii	DeepSeek-R1-Distill-1.5B	1.0120	2.2487	1.4996	9.1955	0.99984	7.9032	0.9154
iviarcii	TinyLlama-v1.1	1.0384	2.3429	1.5306	9.4284	0.99983	8.1317	0.9119
	TinyLlama-1.1B-Chat-v1.0	0.9774	2.2102	1.4867	8.8269	0.99984	7.7688	0.9169
	Pythia-1B	0.9966	2.0688	1.4383	9.3237	0.99985	8.3512	0.9222
	LLaMA3.2-1B	1.1285	3.0418	1.7441	12.2291	0.99981	7.7010	0.8594
	LLaMA3.2-1B-Instruct	0.9483	2.2204	1.4901	10.9033	0.99986	6.7337	0.8974
	Qwen2.5-1.5B	1.1678	3.2390	1.7997	12.4321	0.99980	8.7932	0.8503
April	Qwen2.5-1.5B-Instruct	1.4183	4.1012	2.0251	14.5600	0.99975	9.9183	0.8105
•	DeepSeek-R1-Distill-1.5B	1.1252	2.9771	1.7254	12.1800	0.99982	7.8894	0.8624
	TinyLlama-v1.1	1.1138	3.0726	1.7529	12.0094	0.99981	7.8906	0.8580
April	TinyLlama-1.1B-Chat-v1.0	1.0918	2.8578	1.6905	11.7179	0.99982	8.1742	0.8679
	Pythia-1B	0.9781	2.4767	1.5738	11.1960	0.99985	6.7553	0.8856
	LLaMA3.2-1B	0.9708	2.3205	1.5233	10.3333	0.99983	7.2112	0.9155
	LLaMA3.2-1B-Instruct	0.9294	2.1616	1.4702	9.9291	0.99984	6.5563	0.9213
	Qwen2.5-1.5B	1.0664	2.8976	1.7022	10.9505	0.99979	7.4380	0.8945
May	Qwen2.5-1.5B-Instruct	1.0979	3.0247	1.7392	11.2851	0.99978	7.6943	0.8899
,	DeepSeek-R1-Distill-1.5B	1.0504	2.8495	1.6880	10.9981	0.99979	7.5171	0.8963
	TinyLlama-v1.1	0.9860	2.4176	1.5549	10.3540	0.99982	6.9338	0.9120
	TinyLlama-1.1B-Chat-v1.0		2.6750	1.6356	11.0431	0.99980	7.6696	0.9026
	Pythia-1B	0.9790	2.2545	1.5015	10.5039	0.99983	7.2104	0.9179
	LLaMA3.2-1B	1.0609	2.9319	1.7123	13.2001	0.99978	7.7398	0.8965
	LLaMA3.2-1B-Instruct	0.9669	2.2254	1.4918	12.2753	0.99983	7.0361	0.9214
	Qwen2.5-1.5B	1.1983	3.6029	1.8981	14.3700	0.99973	8.9778	0.8728
June	Qwen2.5-1.5B-Instruct	1.4008	4.6358	2.1531	15.9640	0.99965	10.2455	0.8363
	DeepSeek-R1-Distill-1.5B	1.0752	3.0417	1.7440	13.1595	0.99977	7.3740	0.8926
	TinyLlama-v1.1	1.0048	2.3494	1.5328	12.5272	0.99982	7.1316	0.9170
	TinyLlama-1.1B-Chat-v1.0	1.0800	2.8636	1.6922	13.3478	0.99978	7.7455	0.8989
	Pythia-1B	0.9670	2.1730	1.4741	12.4024	0.99984	6.9883	0.9233

 $<sup>^{\</sup>downarrow}$  Lower is better,  $^{\uparrow}$  Higher is better.

Table 6
Model Performance Metrics for Q3-Q4 (July–December)

Month	Model	MAE↓	MSE↓	RMSE↓	$SMAPE_D^{\downarrow}$	$R_{\scriptscriptstyle D}^{\scriptscriptstyle 2\uparrow}$	$SMAPE_{\Delta t}^{}^{\downarrow}$	$R_{\Delta t}^2{}^\uparrow$
	LLaMA3.2-1B	1.0013	2.3414	1.5302	11.9827	0.99981	7.5753	0.9056
	LLaMA3.2-1B-Instruct	0.9779	2.0390	1.4279	11.8794	0.99983	7.3058	0.9178
	Qwen2.5-1.5B	1.2220	3.7145	1.9273	13.7401	0.99970	8.6895	0.8502
July	Qwen2.5-1.5B-Instruct	1.0961	2.9431	1.7156	13.2183	0.99976	7.9123	0.8813
July	DeepSeek-R1-Distill-1.5B	1.0931	2.5127	1.5851	13.2139	0.99980	7.8593	0.8986
	TinyLlama-v1.1	1.0093	2.2665	1.5055	12.3198	0.99982	7.5489	0.9086
	TinyLlama-1.1B-Chat-v1.0	1.0159	2.1691	1.4728	12.1190	0.99982	8.0089	0.9125
	Pythia-1B	0.9868	2.1418	1.4635	12.1528	0.99983	7.5604	0.9136
	LLaMA3.2-1B	1.0349	2.5877	1.6086	12.5538	0.99976	7.2465	0.9071
	LLaMA3.2-1B-Instruct	0.9675	2.2742	1.5080	12.1986	0.99979	6.5976	0.9183
	Qwen2.5-1.5B	1.2848	3.9831	1.9958	14.7317	0.99963	9.8714	0.8570
August	Qwen2.5-1.5B-Instruct	1.3044	4.5557	2.1344	15.0162	0.99958	8.9693	0.8364
August	DeepSeek-R1-Distill-1.5B	1.0830	3.1092	1.7633	12.8727	0.99971	7.5807	0.8884
	TinyLlama-v1.1	1.0350	2.6723	1.6347	12.6425	0.99975	7.1527	0.9040
	TinyLlama-1.1B-Chat-v1.0	1.0400	2.8707	1.6943	12.8569	0.99973	7.3788	0.8969
	Pythia-1B	1.0538	2.6711	1.6343	13.0296	0.99975	7.3680	0.9041
	LLaMA3.2-1B	0.9571	2.1990	1.4829	11.0576	0.99979	8.4002	0.9224
	LLaMA3.2-1B-Instruct	0.8721	1.8700	1.3675	10.3723	0.99982	6.8206	0.9340
	Qwen2.5-1.5B	1.0753	2.8478	1.6875	12.1321	0.99973	8.6854	0.8995
September	Qwen2.5-1.5B-Instruct	1.0798	2.6380	1.6242	11.9620	0.99975	9.2549	0.9069
September	DeepSeek-R1-Distill-1.5B	0.9814	2.3100	1.5199	11.3042	0.99978	7.7500	0.9185
	TinyLlama-v1.1	0.9202	2.1347	1.4610	10.7115	0.99980	7.6250	0.9247
	TinyLlama-1.1B-Chat-v1.0	0.9475	2.0498	1.4317	10.8078	0.99981	8.0965	0.9277
	Pythia-1B	0.9322	2.1866	1.4787	10.6819	0.99979	7.8955	0.9229
	LLaMA3.2-1B	0.9448	2.0228	1.4222	12.5445	0.99967	8.4875	0.9254
	LLaMA3.2-1B-Instruct	0.8931	1.8767	1.3699	11.5245	0.99969	7.1497	0.9308
	Qwen2.5-1.5B	1.0271	2.7741	1.6656	12.6564	0.99954	8.1672	0.8977
October	Qwen2.5-1.5B-Instruct	1.2379	4.2722	2.0669	14.6202	0.99929	10.0358	0.8424
	DeepSeek-R1-Distill-1.5B	1.0357	2.5105	1.5844	12.9461	0.99959	8.3069	0.9074
	TinyLlama-v1.1	0.9607	2.2818	1.5106	12.4053	0.99962	8.3639	0.9159
	TinyLlama-1.1B-Chat-v1.0	0.9608	2.0309	1.4251	11.8308	0.99966	7.9350	0.9251
	Pythia-1B	0.9059	1.8919	1.3755	11.5062	0.99969	7.3428	0.9302
	LLaMA3.2-1B	0.9526	2.1269	1.4584	12.1783	0.99965	7.3662	0.9252
	LLaMA3.2-1B-Instruct	0.8932	1.7821	1.3350	11.4918	0.99970	7.4177	0.9373
	Qwen2.5-1.5B	1.0650	2.4397	1.5620	13.3018	0.99959	8.1777	0.9141
November	Qwen2.5-1.5B-Instruct	1.0648	2.5090	1.5840	13.3741	0.99958	8.5437	0.9117
	DeepSeek-R1-Distill-1.5B	1.0128	2.2492	1.4997	12.6010	0.99963	7.9037	0.9209
	TinyLlama-v1.1	0.9379 0.9117	1.9974	1.4133	12.1604	0.99967	7.5292	0.9297
	TinyLlama-1.1B-Chat-v1.0			1.3723	11.8652	0.99969	7.8927	0.9338
	Pythia-1B	0.8835	1.7301	1.3153	11.7209	0.99971	7.1682	0.9391
	LLaMA3.2-1B	0.9156	1.7595	1.3265	12.7216	0.99982	7.0403	0.9330
	LLaMA3.2-1B-Instruct	0.8934 1.6067	1.6342	1.2784	12.9921	0.99983	<b>6.4888</b>	0.9378
	Qwen2.5-1.5B Qwen2.5-1.5B-Instruct	1.6067	4.8744	2.2078	19.2261	0.99950	11.1006	0.8145
December		1.3777	4.3643	2.0891	17.3179	0.99955 0.99978	9.7979	0.8339
	DeepSeek-R1-Distill-1.5B	1.0280	2.1739	1.4744	13.7969		7.2068	0.9173
	TinyLlama-v1.1	1.0832	2.5549	1.5984	14.6752 13.5706	0.99974	8.2762 6.7434	0.9028
	TinyLlama-1.1B-Chat-v1.0 Pythia-1B	0.9577 0.9285	1.8877 1.8230	1.3739 1.3502	13.5796 13.1617	0.99981 0.99981	6.7434 6.7443	0.9282 0.9306
	Htter † Higher is hetter	0.9203	1.0230	1.5502	13.1017	0.99901	0.1443	0.5300

 $<sup>\</sup>downarrow$  Lower is better,  $\uparrow$  Higher is better.

**Table 7** Model Performance for Q1 (January–March)

Month	Model	MAE↓	MSE↓	RMSE↓	$SMAPE_D^{\downarrow}$	$R_{\scriptscriptstyle D}^{\scriptscriptstyle 2\uparrow}$	$SMAPE_{\Delta t}^{\downarrow}$	$R^2_{\Delta t}$
	Full Context	0.9074	2.1798	1.4764	7.7226	0.99991	7.5289	0.9136
	Without Textual Information	1.0977	2.8337	1.6834	9.2716	0.99988	9.6124	0.8877
	Without Flight Information	0.9049	2.0748	1.4404	7.8173	0.99991	8.3820	0.9178
lanuary	Without Weather Information	1.1516	3.0966	1.7597	9.5516	0.99987	9.7125	0.8773
January	Without METAR	0.9109	2.0230	1.4223	7.7339	0.99991	7.7235	0.9198
	Without TAF	0.8787	1.9071	1.3810	7.3968	0.99992	7.7284	0.9244
	Without NOTAMs	1.3565	3.9314	1.9828	10.8599	0.99983	11.0969	0.8442
	Without All Trajectories	2.4455	12.7980	3.5774	16.7755	0.99946	22.4854	0.4927
	Without Focusing Trajectory	1.1938	3.1098	1.7635	9.8255	0.99987	12.2782	0.8767
	Without Active Trajectories	0.9296	2.2951	1.5150	8.2534	0.99990	8.1610	0.9090
	Without Prior Trajectories	1.2892	3.7040	1.9246	10.9643	0.99984	10.9403	0.8532
	Full Context	0.9023	1.7515	1.3234	8.6933	0.99990	8.3369	0.9358
	Without Textual Information	0.9457	1.8088	1.3449	9.3358	0.99989	8.6091	0.9337
	Without Flight Information	0.8054	1.5574	1.2480	8.1958	0.99991	7.6528	0.9429
February	Without Weather Information	0.8104	1.3630	1.1675	8.0553	0.99992	7.3063	0.9501
rebruary	Without METAR	1.0812	2.3881	1.5454	10.2895	0.99986	9.9683	0.9125
	Without TAF	0.8408	1.4357	1.1982	8.1196	0.99992	7.8462	0.9474
	Without NOTAMs	0.7789	1.2568	1.1211	7.9574	0.99993	6.6601	0.9540
	Without All Trajectories	3.1719	19.9589	4.4675	22.8117	0.99883	29.1812	0.2688
	Without Focusing Trajectory	1.4247	4.1994	2.0492	12.3865	0.99975	15.9053	0.8462
	Without Active Trajectories	1.1284	2.4138	1.5537	10.8637	0.99986	9.4770	0.9116
	Without Prior Trajectories	1.1932	2.7324	1.6530	10.7404	0.99984	10.6528	0.8999
	Full Context	0.9054	1.9429	1.3939	8.3270	0.99986	7.5979	0.9269
	Without Textual Information	1.0915	2.8445	1.6866	9.8405	0.99980	8.9635	0.8930
	Without Flight Information	0.9191	1.9582	1.3994	8.3935	0.99986	7.2947	0.9264
March	Without Weather Information	0.9575	2.1133	1.4537	9.0038	0.99985	7.5829	0.9205
iviaicii	Without METAR	0.9539	2.1857	1.4784	8.8464	0.99984	7.3382	0.9178
	Without TAF	1.0184	2.3494	1.5328	9.2595	0.99983	8.2568	0.9116
	Without NOTAMs	1.2039	3.1883	1.7856	10.4703	0.99977	9.5013	0.8801
	Without All Trajectories	2.7423	15.4991	3.9369	19.6905	0.99889	23.4856	0.4170
	Without Focusing Trajectory	2.8069	19.7132	4.4400	20.7654	0.99859	23.1440	0.2585
	Without Active Trajectories	1.0162	2.3732	1.5405	9.4628	0.99983	8.6576	0.9107
	Without Prior Trajectories	1.0102	2.2177	1.4892	9.3372	0.99984	9.3373	0.9166

<sup>↓</sup> Lower is better, ↑ Higher is better.

# C. Full Context Analysis Results

Table 8
Model Performance for Q2 (April–June)

Month	Model	$MAE^{\downarrow}$	MSE↓	RMSE↓	$SMAPE_D^{\ \downarrow}$	$R_D^2{}^\uparrow$	$SMAPE_{\Delta t}^{\downarrow}$	$R_{\Delta t}^2{}^\uparrow$
	Full Context	0.9483	2.2204	1.4901	10.9033	0.99986	6.7337	0.8974
	Without Textual Information	1.0218	2.6042	1.6138	11.6386	0.99984	7.2961	0.8797
	Without Flight Information	0.9289	2.2644	1.5048	10.9751	0.99986	6.5958	0.8954
۱: ۵ م	Without Weather Information	0.9853	2.4929	1.5789	11.2667	0.99985	6.8435	0.8848
April	Without METAR	0.9639	2.3067	1.5188	11.2155	0.99986	6.7523	0.8934
	Without TAF	1.4467	4.4181	2.1019	14.6432	0.99973	10.9560	0.7959
	Without NOTAMs	0.8963	2.0808	1.4425	10.4439	0.99987	6.4001	0.9038
	Without All Trajectories	2.4288	13.6587	3.6958	21.3268	0.99916	18.2874	0.3689
	Without Focusing Trajectory	2.4582	15.5982	3.9495	21.2149	0.99904	18.3237	0.2793
	Without Active Trajectories	0.9459	2.2794	1.5098	10.9661	0.99986	6.6560	0.8947
	Without Prior Trajectories	1.3311	3.7610	1.9393	14.0949	0.99977	9.6272	0.8262
	Full Context	0.9294	2.1616	1.4702	9.9291	0.99984	6.5563	0.9213
	Without Textual Information	1.0176	2.3380	1.5290	10.6221	0.99983	7.1981	0.9149
	Without Flight Information	0.9368	2.1732	1.4742	10.1804	0.99984	7.1578	0.9209
Mari	Without Weather Information	0.9742	2.1549	1.4680	10.2734	0.99984	7.5117	0.9215
May	Without METAR	0.9574	2.0493	1.4316	10.0460	0.99985	7.4294	0.9254
	Without TAF	1.0062	2.4767	1.5738	10.7096	0.99982	7.2864	0.9098
	Without NOTAMs	0.9029	1.9877	1.4099	9.4669	0.99985	6.9338	0.927
	Without All Trajectories	3.0113	17.8540	4.2254	24.0631	0.99868	23.2055	0.3499
	Without Focusing Trajectory	1.7352	6.7964	2.6070	15.9799	0.99950	14.2820	0.7525
	Without Active Trajectories	0.9798	2.0669	1.4377	10.4690	0.99985	7.2774	0.9247
	Without Prior Trajectories	0.9710	2.3356	1.5283	10.1317	0.99983	7.3870	0.9150
	Full Context	0.9669	2.2254	1.4918	12.2753	0.99983	7.0361	0.9214
	Without Textual Information	0.9924	2.3334	1.5275	12.4934	0.99982	6.9779	0.9176
	Without Flight Information	1.2905	3.8926	1.9730	14.9703	0.99971	8.9481	0.8625
luma	Without Weather Information	1.1042	3.1180	1.7658	13.6114	0.99976	7.3959	0.8899
June	Without METAR	1.0413	2.6701	1.6340	13.0183	0.99980	7.2847	0.9057
	Without TAF	1.0177	2.8125	1.6771	12.3968	0.99979	7.8702	0.9007
	Without NOTAMs	0.9211	1.8717	1.3681	11.7378	0.99986	6.4112	0.9339
	Without All Trajectories	2.9809	18.3495	4.2836	25.6296	0.99861	21.9901	0.3520
	Without Focusing Trajectory	1.3339	4.1165	2.0289	14.6952	0.99969	11.0694	0.8546
	Without Active Trajectories	0.9815	2.2848	1.5115	12.7503	0.99983	6.6159	0.9193
	Without Prior Trajectories	1.0335	2.3063	1.5187	13.0558	0.99983	7.5159	0.9185

Lower is better, ↑ Higher is better.

**Table 9** Model Performance for Q3 (July–September)

Month	Model	MAE↓	MSE↓	RMSE↓	$SMAPE_D^{\downarrow}$	$R_D^{2\uparrow}$	$SMAPE_{\Delta t}^{\downarrow}$	$R_{\Delta t}^{2}$
	Full Context	0.9779	2.0390	1.4279	11.8794	0.99983	7.3058	0.9178
	Without Textual Information	1.0305	2.1855	1.4783	12.6284	0.99982	7.5088	0.9118
	Without Flight Information	0.9766	2.0451	1.4301	12.1323	0.99983	7.3660	0.9175
Lake	Without Weather Information	0.9495	2.0651	1.4371	11.9360	0.99983	6.6536	0.9167
July	Without METAR	0.9866	2.1627	1.4706	12.1123	0.99982	7.2214	0.9128
Month  July  August	Without TAF	1.0063	2.2215	1.4905	12.3320	0.99982	7.4820	0.9104
	Without NOTAMs	0.9151	1.9631	1.4011	11.5509	0.99984	6.8400	0.9208
	Without All Trajectories	2.9250	18.8846	4.3456	25.9644	0.99846	21.7617	0.2382
	Without Focusing Trajectory	1.2792	3.6322	1.9058	13.9341	0.99970	11.2865	0.8535
	Without Active Trajectories	0.9996	2.2389	1.4963	12.2851	0.99982	7.9943	0.9097
	Without Prior Trajectories	0.9825	2.0861	1.4443	12.2267	0.99983	6.9645	0.9159
	Full Context	0.9675	2.2742	1.5080	12.1986	0.99979	6.5976	0.9183
	Without Textual Information	1.0189	2.5999	1.6124	12.6721	0.99976	7.1502	0.9066
	Without Flight Information	1.0427	2.4984	1.5806	13.0385	0.99977	8.1249	0.9103
A	Without Weather Information	1.0539	2.7081	1.6456	12.9250	0.99975	7.0680	0.9028
August	Without METAR	1.0057	2.6054	1.6141	12.5688	0.99976	6.8738	0.9065
	Without TAF	0.9486	2.3424	1.5305	12.0928	0.99978	6.3984	0.9159
	Without NOTAMs	0.9755	2.3303	1.5265	12.2459	0.99978	6.6143	0.9163
	Without All Trajectories	2.6377	14.8882	3.8585	23.8236	0.99861	20.3841	0.4654
	Without Focusing Trajectory	1.4391	5.0106	2.2384	15.7713	0.99953	11.8805	0.8201
	Without Active Trajectories	1.0491	2.8388	1.6849	12.6682	0.99974	6.9338	0.8981
	Without Prior Trajectories	1.0348	2.6805	1.6372	12.8909	0.99975	7.9558	0.9038
	Full Context	0.8721	1.8700	1.3675	10.3723	0.99982	6.8206	0.9340
	Without Textual Information	0.9505	2.1839	1.4778	11.1034	0.99979	7.8916	0.9230
	Without Flight Information	0.8799	1.8970	1.3773	10.3290	0.99982	7.3468	0.9331
Cantanahau	Without Weather Information	0.9774	2.2235	1.4911	11.2718	0.99979	7.8802	0.9216
September	Without METAR	0.9334	2.0244	1.4228	11.1036	0.99981	7.6207	0.9286
	Without TAF	0.8734	1.9449	1.3946	10.0869	0.99982	7.0707	0.9314
	Without NOTAMs	1.0789	2.4187	1.5552	11.9766	0.99977	9.7979	0.9147
	Without All Trajectories	2.5926	14.4186	3.7972	23.0578	0.99863	23.6338	0.4912
	Without Focusing Trajectory	1.5898	5.7639	2.4008	15.9623	0.99945	15.4688	0.7966
	Without Active Trajectories	0.9780	2.2288	1.4929	11.0431	0.99979	8.0546	0.9214
	Without Prior Trajectories	0.8919	2.0604	1.4354	10.2853	0.99980	7.1557	0.9273

<sup>↓</sup> Lower is better, ↑ Higher is better.

**Table 10**Model Performance for Q4 (October-December)

Month	Model	$MAE^{\downarrow}$	MSE↓	$\textbf{RMSE}^{\downarrow}$	$SMAPE_{D}^{\downarrow}$	$R_D^{2\uparrow}$	$SMAPE_{\Delta t}^{}^{\downarrow}$	$R_{\Delta t}^2{}^\uparrow$
	Full Context	0.8931	1.8767	1.3699	11.5245	0.99969	7.1497	0.9308
	Without Textual Information	1.0133	2.5349	1.5921	12.5664	0.99958	8.0088	0.9065
	Without Flight Information	0.8415	1.7910	1.3383	11.0727	0.99970	6.9427	0.9340
October	Without Weather Information	1.0511	3.0188	1.7375	12.9822	0.99950	8.6614	0.8887
October	Without METAR	0.8497	1.6838	1.2976	11.0734	0.99972	6.7812	0.9379
	Without TAF	0.8852	1.8401	1.3565	11.5888	0.99970	7.1022	0.9321
	Without NOTAMs	0.8630	1.8330	1.3539	11.4442	0.99970	7.1753	0.9324
	Without All Trajectories	2.3656	13.6659	3.6967	22.8737	0.99774	21.1300	0.4961
	Without Focusing Trajectory	1.3790	5.2925	2.3005	15.7475	0.99913	13.4323	0.8049
	Without Active Trajectories	0.8553	1.8187	1.3486	11.3867	0.99970	6.5662	0.9329
	Without Prior Trajectories	1.1746	4.0501	2.0125	14.1528	0.99933	9.3349	0.8507
	Full Context	0.8932	1.7821	1.3350	11.4918	0.99970	7.4177	0.9373
November	Without Textual Information	0.9791	2.1326	1.4603	12.6642	0.99964	7.7896	0.9250
	Without Flight Information	1.2715	3.6552	1.9119	14.4189	0.99939	11.1492	0.8714
	Without Weather Information	0.9327	1.8441	1.3580	12.1507	0.99969	8.0972	0.9351
	Without METAR	0.8983	1.7716	1.3310	11.6085	0.99970	6.9296	0.9377
	Without TAF	0.8672	1.6654	1.2905	11.4647	0.99972	6.9180	0.9414
	Without NOTAMs	0.8392	1.6595	1.2882	11.1810	0.99972	7.1453	0.9416
	Without All Trajectories	2.8065	17.6258	4.1983	27.3398	0.99706	23.3370	0.3800
	Without Focusing Trajectory	1.1871	3.4078	1.8460	14.4316	0.99943	11.9716	0.8801
	Without Active Trajectories	0.9250	1.8833	1.3723	11.9705	0.99969	8.7367	0.9338
	Without Prior Trajectories	0.8404	1.6763	1.2947	11.1934	0.99972	6.6889	0.9410
	Full Context	0.8934	1.6342	1.2784	12.9921	0.99983	6.4888	0.9378
	Without Textual Information	0.9643	1.9332	1.3904	13.1579	0.99980	7.2932	0.9264
	Without Flight Information	0.8881	1.6077	1.2679	12.4841	0.99984	6.9389	0.9388
D	Without Weather Information	0.9299	1.7443	1.3207	13.1765	0.99982	6.5655	0.9336
December	Without METAR	0.8770	1.6226	1.2738	12.5185	0.99983	6.5165	0.9382
	Without TAF	0.9192	1.6872	1.2989	13.0861	0.99983	6.4581	0.9358
	Without NOTAMs	0.7564	1.1624	1.0781	11.3962	0.99988	5.7425	0.9558
	Without All Trajectories	2.7659	19.1522	4.3763	26.3006	0.99804	21.0256	0.2711
	Without Focusing Trajectory	1.3692	4.1613	2.0399	16.7226	0.99957	12.2092	0.8416
	Without Active Trajectories	1.3759	3.9133	1.9782	17.3345	0.99960	9.9423	0.8511
	Without Prior Trajectories	1.3759	3.9133	1.9782	17.3345	0.99960	9.9423	0.8511

Lower is better, ↑ Higher is better.

# **CRediT** authorship contribution statement

**Thaweerath Phisannupawong:** Conceptualization, Data Curation, Formal Analysis, Methodology, Software, Writing – original draft. **Joshua Julian Damanik:** Data Curation, Software, Writing – review and editing. **Han-Lim Choi:** Investigation, Supervision, Validation, Writing – review and editing.

# References

- [1] G. Enea, M. Porretta, A comparison of 4d-trajectory operations envisioned for 'nextgen' and 'sesar', some preliminary findings, in: Proceedings of the 28th Congress of the International Council of the Aeronautical Sciences, 2012, pp. 23–28.
- [2] M. López-Lago, J. Serna, R. Casado, A. Bermúdez, Present and future of air navigation: Pbn operations and supporting technologies, International Journal of Aeronautical and Space Sciences 21 (2) (2019) 451–468. doi:10.1007/s42405-019-00216-y.
- [3] E. Mueller, G. Chatterji, Analysis of aircraft arrival and departure delay characteristics, in: AIAA's Aircraft Technology, Integration, and Operations (ATIO) 2002 Technical Forum, American Institute of Aeronautics and Astronautics, 2002. doi:10.2514/6.2002-5866. URL http://dx.doi.org/10.2514/6.2002-5866
- [4] A. Khanal, R. Bhusal, K. Subbarao, A. Chakravarthy, W. A. Okolo, Gaussian processes for flight delay prediction: Learning a stochastic process, Journal of Aerospace Information Systems 22 (6) (2025) 457–476. doi:10.2514/1.i011539.
  URL http://dx.doi.org/10.2514/1.I011539
- [5] R. Nigam, K. Govinda, Cloud based flight delay prediction using logistic regression, in: 2017 International Conference on Intelligent Sustainable Systems (ICISS), 2017, pp. 662–667. doi:10.1109/ISS1.2017.8389254.
- [6] Q. Li, R. Jing, Z. S. Dong, Flight delay prediction with priority information of weather and non-weather features, IEEE Transactions on Intelligent Transportation Systems 24 (7) (2023) 7149–7165. doi:10.1109/TITS.2023.3270743.
- [7] Y. Tang, Airline flight delay prediction using machine learning models, in: Proceedings of the 2021 5th International Conference on E-Business and Internet, ICEBI '21, Association for Computing Machinery, New York, NY, USA, 2022, p. 151–154. doi:10.1145/3497701.3497725.
- [8] I. Hatıpoğlu, Ö. Tosun, Predictive modeling of flight delays at an airport using machine learning methods, Applied Sciences 14 (13) (2024) 5472.
- [9] M. Alfarhood, R. Alotaibi, B. Abdulrahim, A. Einieh, M. Almousa, A. Alkhanifer, Predicting flight delays with machine learning: A case study from saudi arabian airlines, International Journal of Aerospace Engineering 2024 (2024) 1–12. doi:10.1155/2024/3385463.
- [10] M.-T. Vo, T.-V. Tran, D.-T. Pham, T.-H. Do, A practical real-time flight delay prediction system using big data technology, in: 2022 IEEE International Conference on Communication, Networks and Satellite (COMNETSAT), 2022, pp. 160–167. doi:10.1109/COMNETSAT56033. 2022.9994427.
- [11] W. Shao, A. Prabowo, S. Zhao, S. Tan, P. Koniusz, J. Chan, X. Hei, B. Feest, F. D. Salim, Flight delay prediction using airport situational awareness map, in: Proceedings of the 27th ACM SIGSPATIAL International Conference on Advances in Geographic Information Systems, SIGSPATIAL '19, Association for Computing Machinery, New York, NY, USA, 2019, p. 432–435. doi:10.1145/3347146.3359079.
- [12] W. Wu, K. Cai, Y. Yan, Y. Li, An improved svm model for flight delay prediction, in: 2019 IEEE/AIAA 38th Digital Avionics Systems Conference (DASC), 2019, pp. 1–6. doi:10.1109/DASC43569.2019.9081611.
- [13] B. Yu, Z. Guo, S. Asian, H. Wang, G. Chen, Flight delay prediction for commercial air transport: A deep learning approach, Transportation Research Part E: Logistics and Transportation Review 125 (2019) 203–221. doi:https://doi.org/10.1016/j.tre.2019.03.013.
- [14] Z. Wang, C. Liao, X. Hang, L. Li, D. Delahaye, M. Hansen, Distribution prediction of strategic flight delays via machine learning methods, Sustainability 14 (22) (2022). doi:10.3390/su142215180.
- [15] A. Evangeline, R. C. Joy, A. A. Rajan, Flight delay prediction using different regression algorithms in machine learning, in: 2023 4th International Conference on Signal Processing and Communication (ICSPC), 2023, pp. 262–266. doi:10.1109/ICSPC57692.2023. 10125675
- [16] R. T. Reddy, P. Basa Pati, K. Deepa, S. T. Sangeetha, Flight delay prediction using machine learning, in: 2023 IEEE 8th International Conference for Convergence in Technology (I2CT), 2023, pp. 1–5. doi:10.1109/I2CT57861.2023.10126220.
- [17] Y. J. Kim, S. Choi, S. Briceno, D. Mavris, A deep learning approach to flight delay prediction, in: 2016 IEEE/AIAA 35th Digital Avionics Systems Conference (DASC), 2016, pp. 1–6. doi:10.1109/DASC.2016.7778092.
- [18] G. Gui, F. Liu, J. Sun, J. Yang, Z. Zhou, D. Zhao, Flight delay prediction based on aviation big data and machine learning, IEEE Transactions on Vehicular Technology 69 (1) (2020) 140–150. doi:10.1109/TVT.2019.2954094.
- [19] Q. Li, R. Jing, Flight delay prediction from spatial and temporal perspective, Expert Systems with Applications 205 (2022) 117662. doi:10.1016/j.eswa.2022.117662.
- [20] Q. Li, X. Guan, J. Liu, A cnn-lstm framework for flight delay prediction, Expert Systems with Applications 227 (2023) 120287. doi: 10.1016/j.eswa.2023.120287.
- [21] J. Qu, S. Wu, J. Zhang, Flight delay propagation prediction based on deep learning, Mathematics 11 (3) (2023) 494. doi:10.3390/math11030494.
- [22] K. Cai, Y. Li, Y.-P. Fang, Y. Zhu, A deep learning approach for flight delay prediction through time-evolving graphs, IEEE Transactions on Intelligent Transportation Systems 23 (8) (2022) 11397–11407. doi:10.1109/TITS.2021.3103502.
- [23] X. Shen, J. Chen, R. Yan, A spatial-temporal model for network-wide flight delay prediction based on federated learning, Applied Soft Computing 154 (2024) 111380.
- [24] J. L. Franco, M. V. M. Neto, F. A. Verri, D. R. Amancio, Graph machine learning for flight delay prediction due to holding manouver, arXiv preprint arXiv:2502.04233 (2025).
- [25] T. Chaudhuri, S. Zhang, Y. Zhang, Attention-based deep learning model for flight delay prediction using real-time trajectory, SESAR Innovation Days 2024 (2024).

- [26] A. Vaswani, N. Shazeer, N. Parmar, J. Uszkoreit, L. Jones, A. N. Gomez, L. u. Kaiser, I. Polosukhin, Attention is all you need, in: I. Guyon, U. V. Luxburg, S. Bengio, H. Wallach, R. Fergus, S. Vishwanathan, R. Garnett (Eds.), Advances in Neural Information Processing Systems, Vol. 30, Curran Associates, Inc., 2017.
- [27] A. Radford, K. Narasimhan, T. Salimans, I. Sutskever, et al., Improving language understanding by generative pre-training (2018).
- [28] A. Radford, J. Wu, R. Child, D. Luan, D. Amodei, I. Sutskever, Language models are unsupervised multitask learners, 2019.
- [29] J. Devlin, M.-W. Chang, K. Lee, K. Toutanova, Bert: Pre-training of deep bidirectional transformers for language understanding, in: Proceedings of the 2019 conference of the North American chapter of the association for computational linguistics: human language technologies, volume 1 (long and short papers), 2019, pp. 4171–4186.
- [30] C. Raffel, N. Shazeer, A. Roberts, K. Lee, S. Narang, M. Matena, Y. Zhou, W. Li, P. J. Liu, Exploring the limits of transfer learning with a unified text-to-text transformer, Journal of machine learning research 21 (140) (2020) 1–67.
- [31] T. Brown, B. Mann, N. Ryder, M. Subbiah, J. D. Kaplan, P. Dhariwal, A. Neelakantan, P. Shyam, G. Sastry, A. Askell, S. Agarwal, A. Herbert-Voss, G. Krueger, T. Henighan, R. Child, A. Ramesh, D. Ziegler, J. Wu, C. Winter, C. Hesse, M. Chen, E. Sigler, M. Litwin, S. Gray, B. Chess, J. Clark, C. Berner, S. McCandlish, A. Radford, I. Sutskever, D. Amodei, Language models are few-shot learners, in: H. Larochelle, M. Ranzato, R. Hadsell, M. Balcan, H. Lin (Eds.), Advances in Neural Information Processing Systems, Vol. 33, Curran Associates, Inc., 2020, pp. 1877–1901.
- [32] J. Wei, M. Bosma, V. Y. Zhao, K. Guu, A. W. Yu, B. Lester, N. Du, A. M. Dai, Q. V. Le, Finetuned language models are zero-shot learners, arXiv preprint arXiv:2109.01652 (2021).
- [33] L. Ouyang, J. Wu, X. Jiang, D. Almeida, C. Wainwright, P. Mishkin, C. Zhang, S. Agarwal, K. Slama, A. Ray, et al., Training language models to follow instructions with human feedback, arXiv preprint arXiv:2203.02155 (2022).
- [34] H. Touvron, T. Lavril, G. Izacard, X. Martinet, M.-A. Lachaux, T. Lacroix, B. Rozière, N. Goyal, E. Hambro, F. Azhar, et al., Llama: Open and efficient foundation language models, arXiv preprint arXiv:2302.13971 (2023).
- [35] H. Touvron, L. Martin, K. Stone, P. Albert, A. Almahairi, Y. Babaei, N. Bashlykov, S. Batra, P. Bhargava, S. Bhosale, et al., Llama 2: Open foundation and fine-tuned chat models, arXiv preprint arXiv:2307.09288 (2023).
- [36] A. Grattafiori, A. Dubey, A. Jauhri, A. Pandey, A. Kadian, A. Al-Dahle, A. Letman, A. Mathur, A. Schelten, A. Vaughan, et al., The llama 3 herd of models, arXiv preprint arXiv:2407.21783 (2024).
- [37] A. Q. Jiang, A. Sablayrolles, A. Mensch, C. Bamford, D. S. Chaplot, D. de las Casas, F. Bressand, G. Lengyel, G. Lample, L. Saulnier, L. R. Lavaud, M.-A. Lachaux, P. Stock, T. L. Scao, T. Lavril, T. Wang, T. Lacroix, W. E. Sayed, Mistral 7b, arXiv preprint arXiv:2310.06825 (2023).
- [38] A. Q. Jiang, A. Sablayrolles, A. Roux, A. Mensch, B. Savary, C. Bamford, D. S. Chaplot, D. de las Casas, E. B. Hanna, F. Bressand, G. Lengyel, G. Bour, G. Lample, L. R. Lavaud, L. Saulnier, M.-A. Lachaux, P. Stock, S. Subramanian, S. Yang, S. Antoniak, T. L. Scao, T. Gervet, T. Lavril, T. Wang, T. Lacroix, W. E. Sayed, Mixtral of experts, arXiv preprint arXiv:2401.04088 (2024).
- [39] Gemma Team, Gemma: Open models based on gemini research and technology, arXiv preprint arXiv:2403.08295 (2024).
- [40] Gemma Team, Gemma 2: Improving open language models at a practical size, arXiv preprint arXiv:2408.00118 (2024).
- [41] Gemma Team, Gemma 3 technical report, arXiv preprint arXiv:2503.19786 (2025).
- [42] S. Gunasekar, Y. Zhang, J. Aneja, C. C. T. Mendes, A. D. Giorno, S. Gopi, M. Javaheripi, P. Kauffmann, G. de Rosa, O. Saarikivi, A. Salim, S. Shah, H. S. Behl, X. Wang, S. Bubeck, R. Eldan, A. T. Kalai, Y. T. Lee, Y. Li, Textbooks are all you need, arXiv preprint arXiv:2306.11644 (2023)
- [43] M. Javaheripi, S. Bubeck, M. Abdin, J. Aneja, S. Bubeck, C. C. T. Mendes, W. Chen, A. Del Giorno, R. Eldan, S. Gopi, et al., Phi-2: The surprising power of small language models, Microsoft Research Blog (2023).
- [44] M. Abdin, J. Aneja, H. Awadalla, A. Awadallah, A. A. Awan, N. Bach, A. Bahree, A. Bakhtiari, J. Bao, H. Behl, A. Benhaim, M. Bilenko, J. Bjorck, S. Bubeck, M. Cai, Q. Cai, V. Chaudhary, D. Chen, D. Chen, W. Chen, Y.-C. Chen, Y.-L. Chen, H. Cheng, P. Chopra, X. Dai, M. Dixon, R. Eldan, V. Fragoso, J. Gao, M. Gao, M. Gao, A. Garg, A. D. Giorno, A. Goswami, S. Gunasekar, E. Haider, J. Hao, R. J. Hewett, W. Hu, J. Huynh, D. Iter, S. A. Jacobs, M. Javaheripi, X. Jin, N. Karampatziakis, P. Kauffmann, M. Khademi, D. Kim, Y. J. Kim, L. Kurilenko, J. R. Lee, Y. T. Lee, Y. Li, Y. Li, C. Liang, L. Liden, X. Lin, Z. Lin, C. Liu, L. Liu, M. Liu, W. Liu, X. Liu, C. Luo, P. Madan, A. Mahmoudzadeh, D. Majercak, M. Mazzola, C. C. T. Mendes, A. Mitra, H. Modi, A. Nguyen, B. Norick, B. Patra, D. Perez-Becker, T. Portet, R. Pryzant, H. Qin, M. Radmilac, L. Ren, G. de Rosa, C. Rosset, S. Roy, O. Ruwase, O. Saarikivi, A. Saied, A. Salim, M. Santacroce, S. Shah, N. Shang, H. Sharma, Y. Shen, S. Shukla, X. Song, M. Tanaka, A. Tupini, P. Vaddamanu, C. Wang, G. Wang, L. Wang, S. Wang, Y. Wang, R. Ward, W. Wen, P. Witte, H. Wu, X. Wu, M. Wyatt, B. Xiao, C. Xu, J. Xu, W. Xu, J. Xue, S. Yadav, F. Yang, J. Yang, Z. Yang, D. Yu, L. Yuan, C. Zhang, C. Zhang, J. Zhang, L. L. Zhang, Y. Zhang, Y. Zhang, Y. Zhang, X. Zhou, Phi-3 technical report: A highly capable language model locally on your phone, arXiv preprint arXiv:2404.14219 (2024).
- [45] Qwen Team, Qwen technical report, arXiv preprint arXiv:2309.16609 (2023).
- [46] Qwen Team, Introducing qwen1.5 (February 2024).
  URL https://qwenlm.github.io/blog/qwen1.5/
- [47] Owen Team, Owen2 technical report, arXiv preprint arXiv:2407.10671 (2024).
- [48] Qwen Team, Qwen2.5 technical report, arXiv preprint arXiv:2412.15115 (2025).
- [49] Qwen Team, Qwen3 technical report, arXiv preprint arXiv:2505.09388 (2025).
- [50] DeepSeek-AI, DeepSeek-r1: Incentivizing reasoning capability in llms via reinforcement learning, arXiv preprint arXiv:2501.12948 (2025).
- [51] X. Olive, L. Basora, B. Viry, R. Alligier, Deep trajectory clustering with autoencoders, in: ICRAT 2020, 9th International Conference for Research in Air Transportation, 2020.
- [52] Z. Yue, Y. Wang, J. Duan, T. Yang, C. Huang, Y. Tong, B. Xu, TS2vec: Towards universal representation of time series, in: Proceedings of the AAAI Conference on Artificial Intelligence, Vol. 36, 2022, pp. 8980–8987.
- [53] X. Zhang, Z. Zhao, T. Tsiligkaridis, M. Zitnik, Self-supervised contrastive pre-training for time series via time-frequency consistency, Advances in neural information processing systems 35 (2022) 3988–4003.

- [54] J. Dong, H. Wu, H. Zhang, L. Zhang, J. Wang, M. Long, Simmtm: A simple pre-training framework for masked time-series modeling, in: A. Oh, T. Naumann, A. Globerson, K. Saenko, M. Hardt, S. Levine (Eds.), Advances in Neural Information Processing Systems, Vol. 36, Curran Associates, Inc., 2023, pp. 29996–30025.
- [55] D. Luo, W. Cheng, Y. Wang, D. Xu, J. Ni, W. Yu, X. Zhang, Y. Liu, Y. Chen, H. Chen, et al., Time series contrastive learning with information-aware augmentations, in: Proceedings of the AAAI Conference on Artificial Intelligence, Vol. 37, 2023, pp. 4534–4542.
- [56] T. Phisannupawong, J. J. Damanik, H.-L. Choi, Aircraft trajectory segmentation-based contrastive coding: A framework for self-supervised trajectory representation, IEEE Open Journal of Intelligent Transportation Systems (2025) 1–1doi:10.1109/0JITS.2025.3574746.
- [57] C. Chang, W.-Y. Wang, W.-C. Peng, T.-F. Chen, Llm4ts: Aligning pre-trained llms as data-efficient time-series forecasters, ACM Trans. Intell. Syst. Technol. 16 (3) (Apr. 2025). doi:10.1145/3719207.
- [58] e. a. Zhou, One fits all: Power general time series analysis by pretrained lm, arXiv preprint arXiv:2302.11939 (2023).
- [59] M. Jin, S. Wang, L. Ma, Z. Chu, J. Y. Zhang, X. Shi, P.-Y. Chen, Y. Liang, Y.-F. Li, S. Pan, Q. Wen, Time-LLM: Time series forecasting by reprogramming large language models, in: International Conference on Learning Representations (ICLR), 2024.
- [60] L. Wang, J. Chou, X. Zhou, A. Tien, D. M. Baumgartner, Aviationgpt: A large language model for the aviation domain, arXiv preprint arXiv:2311.17686 (2023).
- [61] C. Chandra, X. Jing, M. V. Bendarkar, K. Sawant, L. Elias, M. Kirby, D. N. Mavris, Aviation-bert: A preliminary aviation-specific natural language model, in: AIAA AVIATION 2023 Forum, American Institute of Aeronautics and Astronautics, 2023. doi:10.2514/ 6.2023-3436.
- [62] A. Tikayat Ray, O. J. Pinon-Fischer, D. N. Mavris, R. T. White, B. F. Cole, aerobert-ner: Named-entity recognition for aerospace requirements engineering using bert, in: AIAA SciTech 2023 Forum, 2023, p. 2583.
- [63] A. Tikayat Ray, B. F. Cole, O. J. Pinon Fischer, R. T. White, D. N. Mavris, aerobert-classifier: Classification of aerospace requirements using bert, Aerospace 10 (3) (2023) 279.
- [64] G. Moreira, D. Pleffken, W. Santos, C. Cerqueira, M. Gotelip, Using Ilms to automate means of compliance assignment in aerospace defense systems, techrxiv preprint techrxiv: 173156107.77200429/v1 (Nov. 2024).
- [65] S. Abdulhak, W. Hubbard, K. Gopalakrishnan, M. Z. Li, Chatatc: Large language model-driven conversational agents for supporting strategic air traffic flow management, arXiv preprint arXiv:2402.14850 (2024).
- [66] A. Tabrizian, P. Gupta, A. Taye, J. Jones, E. Thompson, S. Chen, T. Bonin, D. Eberle, P. Wei, Using large language models to automate flight planning under wind hazards, in: 2024 AIAA DATC/IEEE 43rd Digital Avionics Systems Conference (DASC), 2024, pp. 1–8. doi:10.1109/DASC62030.2024.10749512.
- [67] W. Zhou, J. Wang, L. Zhu, Y. Wang, Y. Ji, Flight arrival scheduling via large language model, Aerospace 11 (10) (2024) 813.
- [68] J. Andriuškevičius, J. Sun, Automatic control with human-like reasoning: Exploring language model embodied air traffic agents, arXiv preprint arXiv:2409.09717 (2024).
- [69] J. M. Hoekstra, J. Ellerbroek, Bluesky at simulator project: an open data and open source approach, in: Proceedings of the 7th international conference on research in air transportation, Vol. 131, FAA/Eurocontrol Washington, DC, USA, 2016, p. 132.
- [70] D. Guo, E. Q. Wu, Y. Wu, J. Zhang, R. Law, Y. Lin, Flightbert: Binary encoding representation for flight trajectory prediction, IEEE Transactions on Intelligent Transportation Systems 24 (2) (2023) 1828–1842. doi:10.1109/TITS.2022.3219923.
- [71] D. Guo, Z. Zhang, Z. Yan, J. Zhang, Y. Lin, Flightbert++: A non-autoregressive multi-horizon flight trajectory prediction framework, Proceedings of the AAAI Conference on Artificial Intelligence 38 (1) (2024) 127-134. doi:10.1609/aaai.v38i1.27763.
- [72] K. Luo, J. Zhou, Large language models for single-step and multi-step flight trajectory prediction, arXiv preprint arXiv:2501.17459 (2025).
- [73] Q. Zhang, J. H. Mott, An exploratory assessment of llms' potential for flight trajectory reconstruction analysis, Mathematics (2025).
- [74] D. Guo, Z. Zhang, B. Yang, J. Zhang, H. Yang, Y. Lin, Integrating spoken instructions into flight trajectory prediction to optimize automation in air traffic control, Nature Communications 15 (1) (Nov. 2024). doi:10.1038/s41467-024-54069-5.
- [75] Ministry of Land, Infrastructure and Transport, South Korea, Airportal, Electronic resource, accessed: April 7, 2023 (2024).
  URL https://www.airportal.go.kr/
- [76] D. W. Wragg, A dictionary of aviation, p. 189 (1973).
- [77] I. C. A. Organization, PANS-ATM Doc 4444: Procedures for Air Navigation Services Air Traffic Management, sixteenth Edition, ICAO, 2016, https://www.icao.int.
- [78] G. B. Valor, Ogimet: Weather data portal, https://www.ogimet.com/home.phtml.en, accessed: 2025-06-09 (2025).
- [79] Ministry of Land, Infrastructure and Transport, Aeronautical Information Management (AIM), https://aim.koca.go.kr/xNotam/, accessed: 2025-06-09 (2025).
- [80] M. Schäfer, M. Strohmeier, V. Lenders, I. Martinovic, M. Wilhelm, Bringing up opensky: A large-scale ads-b sensor network for research, in: Proceedings of the 13th IEEE/ACM International Symposium on Information Processing in Sensor Networks, 2014, pp. 83–94.
- [81] E. Axell, P. Johansson, M. Alexandersson, J. Rantakokko, Estimation of the position error in gps receivers, FOI-R-3840-SE E36044, Swedish Defence Research Agency (FOI), approved by Christian Jönsson (February 2014).
- [82] A. Haviv, O. Ram, O. Press, P. Izsak, O. Levy, Transformer language models without positional encodings still learn positional information, in: Y. Goldberg, Z. Kozareva, Y. Zhang (Eds.), Findings of the Association for Computational Linguistics: EMNLP 2022, Association for Computational Linguistics, 2022, pp. 1382–1390. doi:10.18653/v1/2022.findings-emnlp.99.
- [83] T. Phisannupawong, J. J. Damanik, H.-L. Choi, Atfmtraj: Aircraft trajectory classification data for air traffic management, https://huggingface.co/datasets/petchthwr/ATFMTraj (2024).
- [84] R. Girshick, Fast r-cnn, in: 2015 IEEE International Conference on Computer Vision (ICCV), 2015, pp. 1440–1448. doi:10.1109/ICCV. 2015.169.
- [85] E. Performance Review Commission, Performance review report 2024: An assessment of air traffic management in europe, Tech. rep., EUROCONTROL (March 2025).